Chapter 10
Multi-carrier Techniques

Multi-carrier techniques are widely used in wireless LANs and fourth generation cellular systems. Orthogonal frequency division multiplexing (OFDM) is widely used modulation technique in high-rate wireless systems such as IEEE 802.11a/g wireless local area network (WLAN) standard due to its robustness to frequency selective fading. Multiple access with OFDM can be achieved using TDMA or random access approaches. Orthogonal frequency division multiple-access (OFDMA) is an extension of OFDM to accommodate multiple simultaneous users. OFDMA was originally proposed by Sari and Karam for cable television networks [229]. Since then OFDMA has been adopted for the forward channel in 3GPP long term evolution (LTE) and in both the forward and reverse channels for IEEE 802.16e Worldwide Interoperability for Microwave Access (WiMAX) standard.

OFDMA achieves multiple access by dividing the available sub-carriers into mutually exclusive sets that are assigned to distinct users for simultaneous transmission. The orthogonality of the sub-carriers ensures protection against multiple-access interference. There are three basic forms of OFDMA depending on how the sub-carriers are allocated to the users. The first is clustered-carrier OFDMA (CC-OFDMA) where each user is allocated a contiguous group of sub-carriers. The second is spaced-carrier OFDMA (SC-OFDMA) where each user is assigned a group of sub-carriers that is regularly spaced across the channel bandwidth. The last is random interleaving OFDMA (RI-OFDMA) where sub-carriers are assigned in a random fashion to each user.

OFDMA has essentially the same advantages and disadvantages as OFDM when compared to single-carrier modulation schemes. It achieves robustness to frequency-selective fading using closely spaced orthogonal sub-carriers, such that frequency-domain equalization (FDE) can be used. However, it also suffers from a high peak-to-average power ratio (PAPR) that requires the use of either PAPR reduction techniques or a highly linear power amplifier. OFDMA is attractive for use on the forward link of a cellular system, since all forward link transmissions can all use the same RF local oscillator and sample clock reference in their digital-to-analog converters (DACs). However, the use of OFDMA on the cellular reverse link

G.L. Stüber, *Principles of Mobile Communication*, DOI 10.1007/978-1-4614-0364-7_10, 583

is complicated considerably by the fact that waveform received at the BS from each MS will have a different carrier frequency offset, timing offset, and sampling clock offset.

To overcome the difficulties of using OFDMA on the cellular reverse link, a modified form of OFDMA, called single-carrier frequency division multiple access (SC-FDMA) was introduced by Myung, Lim and Goodman [189]. SC-FDMA can be viewed as DFT-spread OFDMA, where a block of time-domain data symbols are first transformed to the frequency-domain using a discrete Fourier transform (DFT) before being applied to an OFDMA modulator. Similar to OFDMA, multiple access is achieved by assigning the users disjoint sets of sub-carriers. This can be done using localized FDMA (L-FDMA) where contiguous sub-carriers are assigned to a particular user, or interleaved FDMA (I-FDMA) where users are assigned regularly spaced sub-carriers that are distributed over the entire bandwidth. The resulting SC-FDMA waveform is a single-carrier modulated waveform having a characteristically much lower PAPR than the corresponding multi-carrier OFDMA waveform. This lower PAPR benefits the MS in terms of transmit power efficiency, thereby making SC-FDMA very attractive for the cellular reverse link. For this reason SC-FDMA has been adopted as the reverse channel multiple access scheme for 3GPP LTE.

Section 10.1 begins the chapter with a discussion of OFDM on frequency-selective channels, and describes how a cyclic guard interval can be used to completely remove any intersymbol interference (ISI) in a very efficient fashion, provided that the length of the cyclic guard interval is at least as long as the length of the overall discrete-time channel impulse response. We then consider the performance of OFDM on static ISI channels and fading ISI channels, in cases where the length of the guard interval is less than the length of the overall discrete-time channel impulse response. In this case, residual ISI is present which is shown to be devastating to the performance of OFDM. Section 10.1.2 then presents an effective technique to mitigate residual ISI, called residual ISI cancelation (RISIC) that uses a combination of tail cancelation and cyclic reconstruction. Section 10.2 then considers the combination of single-carrier modulation with FDE, a technique known as single-carrier frequency-domain equalization (SC-FDE). FDE is especially attractive on channels having long impulse responses where the complexity of time-domain equalizers can become prohibitive. Afterwards, Sect. 10.3 treats a variety of issued related to OFDMA. The use of OFDMA on both the forward and reverse link is covered, and issues such as sub-carrier allocation and time-domain windowing are considered. Section 10.4 concludes the chapter with SC-FDMA, including multiplexing methods and analysis of PAPR.

10.1 Orthogonal Frequency Division Multiplexing

Consider an OFDM system where the number of sub-carriers N is chosen to be large enough so that the channel transfer function $T(t, f)$ is essentially constant across sub-bands of width $1/T$. Then

$$T(t,k) \doteq T(t,k\Delta_f), \quad k\Delta_f - 1/(2T) \le f \le k\Delta_f + (1/(2T) \tag{10.1}$$

and no equalization is necessary because the ISI is negligible. Viewing the problem another way, if the block length N is chosen so that $N \gg L$, where L is the length of the discrete-time channel impulse response, then the ISI will only affect a small fraction of the symbol transmitted on each sub-carrier. Weinstein and Ebert [280] came up with an ingenious solution, whereby they inserted a guard interval in the form of a length-G cyclic prefix or cyclic suffix to each IDFT output vector $\mathbf{X}_n = \{X_{n,m}\}$. In fact, if the discrete-time channel impulse response has duration $L \le G$, their method can completely remove the ISI in a very efficient fashion as we now describe.

Suppose that the IDFT output vector $\mathbf{X}_n = \{X_{n,m}\}_{m=0}^{N-1}$ is appended with a cyclic suffix to yield the vector $\mathbf{X}_n^g = \{X_{n,m}^g\}_{m=0}^{N+G-1}$, where

$$X_{n,m}^g = X_{n,(m)_N} \tag{10.2}$$

$$= A \sum_{k=0}^{N-1} x_{\mathrm{n},k} \mathrm{e}^{\frac{\mathrm{j}2\pi km}{N}}, \quad m = 0,\ 1,\ \ldots,\ N+G-1, \tag{10.3}$$

G is the length of the guard interval in samples, and $(m)_N$ is the residue of m modulo N. To maintain the data rate $R_s = 1/T_{\mathrm{s}}$, the DAC in the transmitter is clocked with rate $R_s^g = \frac{N+G}{N} R_s$, due to the insertion of the cyclic guard interval.

Consider a time-invariant ISI channel with impulse response $g(t)$. The combination of the DAC, waveform channel $g(t)$, anti-aliasing filter, and DAC yields an overall discrete-time channel with sampled impulse response $\mathbf{g} = \{g_m\}_{m=0}^{L}$, where L is the length of the discrete-time channel impulse response. The discrete-time linear convolution of the transmitted sequence $\{\mathbf{X}_n^g\}$ with the discrete-time channel produces the discrete-time received sequence $\{R_{n,m}^g\}$, where

$$R_{n,m}^g = \begin{cases} \sum_{i=0}^{m} g_i X_{n,m-i}^g + \sum_{i=m+1}^{L} g_i X_{n-1,N+G+m-i}^g + \tilde{n}_{n,m}, & 0 \le m < L, \\ \sum_{i=0}^{L} g_i X_{n,m-i}^g + \tilde{n}_{n,m}, & L \le m \le N+G-1. \end{cases} \tag{10.4}$$

To remove the ISI introduced by the channel, the first G received samples $\{R_{n,m}^g\}_{m=0}^{G-1}$ are discarded and replaced with the last G received samples $\{R_{n,m}^g\}_{m=N}^{N+G-1}$, as shown in Fig. 10.1. If the length of the guard interval satisfies $G \ge L$, then we obtain the received sequence

$$R_{n,m} = R_{n,G+(m-G)_N}^g$$

$$= \sum_{i=0}^{L} g_i X_{n,(m-i)_N} + \tilde{n}_{n,(m-i)_N}, \quad 0 \le m \le N-1. \tag{10.5}$$

Note that the first term in (10.5) represents a circular convolution of the transmitted sequence $\mathbf{X}_n = \{X_{n,m}\}$ with the discrete-time channel $\mathbf{g} = \{g_m\}_{m=0}^{L}$.

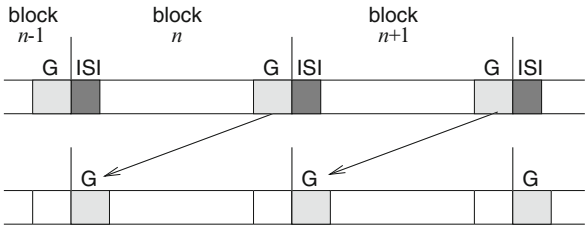

Fig. 10.1 Removal of ISI using the cyclic suffix

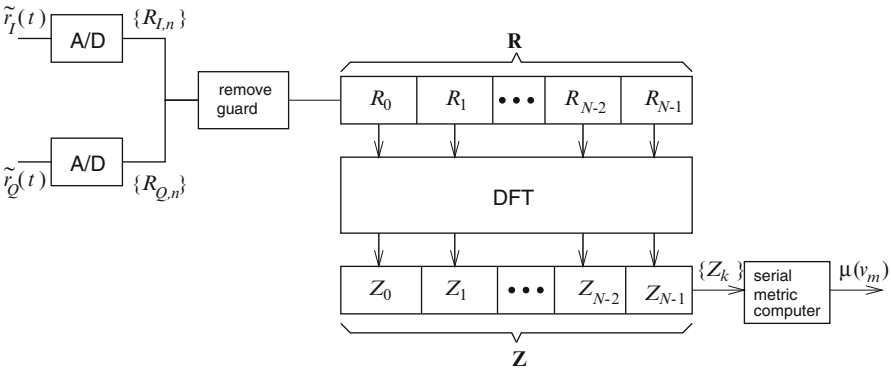

Fig. 10.2 Block diagram of OFDM receiver

As shown in Fig. 10.2, the OFDM baseband demodulator computes the DFT of the vector $\mathbf{R}_n$. This yields the output vector

$$\begin{aligned} z_{n,i} &= \frac{1}{N}\sum_{m=0}^{N-1} R_{n,m} \mathrm{e}^{-\mathrm{j}\frac{2\pi mi}{N}} \\ &= T_i A x_{\mathrm{n},i} + v_{n,i}, \quad 0 \le i \le N-1, \end{aligned} \tag{10.6}$$

where

$$T_i = \sum_{m=0}^{L} g_m \mathrm{e}^{-\mathrm{j}\frac{2\pi mi}{N}} \tag{10.7}$$

and the noise samples $\{v_{n,i}\}$ are i.i.d complex Gaussian random variables with zero-mean and variance $N_0/(NT_s^g)$. Note that $\mathbf{T} = \{T_i\}_{i=0}^{N-1}$ is the DFT of the zero-padded sequence $\mathbf{g} = \{g_m\}_{m=0}^{N-1}$ and is equal to the sampled frequency response of the channel. To be consistent with our earlier results in Chap. 5, we can multiply the $z_{n,i}$ for convenience by the scalar $\sqrt{NT_s^g}$. By following the same argument used in Sect. 5.7, such scaling gives

$$\tilde{z}_{n,i} = T_i \hat{A} x_{\mathrm{n},i} + \tilde{v}_{n,i} \quad i = 0, \ldots, N-1, \tag{10.8}$$

where $\hat{A} = \sqrt{2E_hN/(N+G)}$ and the $\tilde{v}_{n,i}$ are i.i.d. zero-mean Gaussian random variables with variance N_0. Note that in this case, E_h is defined in (4.56). Observe that each $\tilde{z}_{n,i}$ depends only on the corresponding data symbol $x_{\mathrm{n},i}$ and, therefore, the ISI has been completely removed. Once again, for *each* of the $\tilde{z}_{n,i}$, the receiver decides in favor of the *signal vector* $\tilde{\mathbf{s}}_m$ that minimizes the squared Euclidean distance

$$\mu(\tilde{s}_m) = \|\tilde{z}_{n,i} - T_i\hat{A}x_{\mathrm{n},i}\|^2. \tag{10.9}$$

Thus, for each OFDM block, N symbol decisions must be made, one for each of the N sub-carriers.

10.1.1 Performance of OFDM on ISI Channels

For channels having long delay spreads or with deployment of single frequency simulcast networks (SFNs), the possibility exists that duration of the ISI will exceed the length of the guard interval. Such ISI is called *residual* ISI, and is devastating even in small amounts. Increasing the length of guard interval to reduce residual ISI has its limitations, because it introduces bandwidth penalty. An attempt to equalize residual ISI has been suggested in [269], but the technique has high complexity and provides only a limited improvement. This section presents an effective technique to mitigate residual ISI, called RISIC. The RISIC technique is based on a very efficient method for echo cancelation [56]. The RISIC technique can be thought of as an iterative version of the echo cancelation method in [56]. The RISIC technique will be shown to be highly effective for combating residual ISI with reasonable complexity.

10.1.1.1 Static ISI Channels

Once again, in an attempt to remove the ISI introduced by the channel, the first G received samples $\{R^g_{n,m}\}_{m=0}^{G-1}$ in (10.4) are discarded and replaced with the last G received samples $\{R^g_{n,m}\}_{m=N}^{N+G-1}$. If the length of the channel exceeds the length of the guard interval such that $G < L$, then the received samples after removal of the guard interval can be rewritten as the sum of two components, viz.,

$$R_{n,m} = R_{n|n-1,m} + R_{n|n,m}, \tag{10.10}$$

where $R_{n|n-1,m}$ is the received sample component with contributions only from block $n-1$ and $R_{n|n,m}$ is the received sample component with contributions only from block n. Then, in the absence of noise[1]

[1]Here we ignore noise to highlight the effect of ISI.

$$R_{n|n-1,m} = \sum_{i=G+1}^{L} g_i X_{n-1,(m-i)_N}(1-u(m-i+G)), \tag{10.11}$$

$$R_{n|n,m} = \sum_{i=0}^{L} g_i X_{n,(m-i)_N} u(m-i+G), \tag{10.12}$$

where $u(n)$ is the unit step function. The received sample sequence $\{R_{n,m}\}_{m=0}^{N-1}$ is demodulated by taking the N-point DFT

$$\mathrm{DFT}\{R_{n,m}\} = \mathrm{DFT}\{R_{n|n-1,m}\} + \mathrm{DFT}\{R_{n|n,m}\}. \tag{10.13}$$

We can express $\mathrm{DFT}\{R_{n|n-1,m}\}$ as

$$\frac{1}{N}\sum_{i=G+1}^{L} g_i \sum_{\ell=0}^{N-1} x_{\mathrm{n}-1,\ell} \exp\left\{-\mathrm{j}\frac{2\pi\ell i}{N}\right\} \sum_{m=0}^{N-1} u(i-m-G-1) \exp\left\{\mathrm{j}\frac{2\pi(\ell-k)m}{N}\right\} \tag{10.14}$$

and $\mathrm{DFT}\{R_{n|n,m}\}$ by

$$\begin{aligned} & x_{\mathrm{n},k}\left\{\sum_{i=0}^{G} g_i \exp\left\{-\mathrm{j}\frac{2\pi ki}{N}\right\} + \sum_{i=G+1}^{L} g_i \exp\left\{-\mathrm{j}\frac{2\pi ki}{N}\right\}\left(1+\frac{G}{N}-\frac{i}{N}\right)\right\} \\ & -\frac{1}{N}\sum_{i=G+1}^{L} g_i \sum_{\substack{l=0 \\ \ell\neq k}}^{N-1} x_{\mathrm{n},\ell} \exp\left\{-\mathrm{j}\frac{2\pi\ell i}{N}\right\} \sum_{m=0}^{N-1} u(i-m-G-1) \exp\left\{\mathrm{j}\frac{2\pi(\ell-k)m}{N}\right\}. \end{aligned} \tag{10.15}$$

For symbol k of block n, (10.14) is the ISI contribution from block $n-1$, the top half of (10.15) is the useful signal term, and the bottom half of (10.15) is the ICI term. We can express (10.13) as

$$z_{n,k} = \mathrm{DFT}\{R_{n,m}\} \tag{10.16}$$

$$= \eta_k x_{\mathrm{n},k} + I_k, \tag{10.17}$$

where

$$\eta_k = \sum_{i=0}^{G} g_i \exp\left\{-\mathrm{j}\frac{2\pi ki}{N}\right\} + \sum_{i=G+1}^{L} g_i \exp\left\{-\mathrm{j}\frac{2\pi ki}{N}\right\}\left(1+\frac{G}{N}-\frac{i}{N}\right), \tag{10.18}$$

$$I_k = I_{n,k} + I_{n-1,k} \tag{10.19}$$

and where $I_{n,k}$ the ICI term and $I_{n-1,k}$ the ISI term.

Next we find the signal-to-interference ratio (SIR) for symbol k defined by

$$\mathrm{SIR}(k) = E_u(k)/E_I(k), \tag{10.20}$$

where the useful signal energy is

$$E_u(k) = \frac{1}{2}\mathrm{E}|\eta_k x_{\mathrm{n},k}|^2. \tag{10.21}$$

Since the input symbols $\{x_{\mathrm{n},k}\}$ are assumed independent, $x_{\mathrm{n},k}$ and I_k are also independent. Furthermore, $I_{n,k}$ and $I_{n-1,k}$ are independent, too. Then, interference energy is

$$\begin{aligned} E_I(k) &= \frac{1}{2}\mathrm{E}|I_k|^2 \\ &= \frac{1}{2}\mathrm{E}|I_{n-1,k}|^2 + \frac{1}{2}\mathrm{E}|I_{n,k}|^2 \\ &= E_{\mathrm{ISI}}(k) + E_{ICI}(k). \end{aligned} \tag{10.22}$$

The signal energy in (10.21) can be expressed as

$$\begin{aligned} E_u(k) &= E_s \left| \sum_{i=0}^{G} g_i \exp\left\{-\mathrm{j}\frac{2\pi ki}{N}\right\} + \sum_{i=G+1}^{L} g_i \exp\left\{-\mathrm{j}\frac{2\pi ki}{N}\right\}\left(1 + \frac{G}{N} - \frac{i}{N}\right)\right|^2 \\ &\approx E_s \left| \sum_{i=0}^{L} g_i \exp\left\{-\mathrm{j}\frac{2\pi ki}{N}\right\}\right|^2, \quad \text{if } L - G << N. \end{aligned} \tag{10.23}$$

From (10.22),

$$\begin{aligned} E_{\mathrm{ISI}}(k) = \frac{E_s}{N}\Bigg\{ &\sum_{i=G+1}^{L}\sum_{i'=i}^{L} 2(i-G)\mathrm{Re}\left\{g_i g_i^* \exp\left\{-\mathrm{j}\frac{2\pi k(i-i')}{N}\right\}\right\} \\ &- \sum_{i=G+1}^{L} |g_i|^2 (i-G)\Bigg\}, \end{aligned} \tag{10.24}$$

$$E_{ICI}(k) = E_{\mathrm{ISI}}(k) - \frac{E_s}{N^2}\left| \sum_{i=G+1}^{L} g_i \exp\left\{-\mathrm{j}\frac{2\pi ki}{N}(i-G)\right\}\right|^2. \tag{10.25}$$

Note that the second term in (10.25) is relatively small when $L - G \ll N$, in which case $E_I(k) \approx 2E_{\mathrm{ISI}}(k)$.

Table 10.1 Four-tap static ISI channel models

tap #	Delay (μs)	Fractional power channel 1	Fractional power channel 2
0	0.0	0.15	0.39
1	0.2	0.65	0.16
2	0.4	0.15	0.26
3	0.6	0.05	0.19

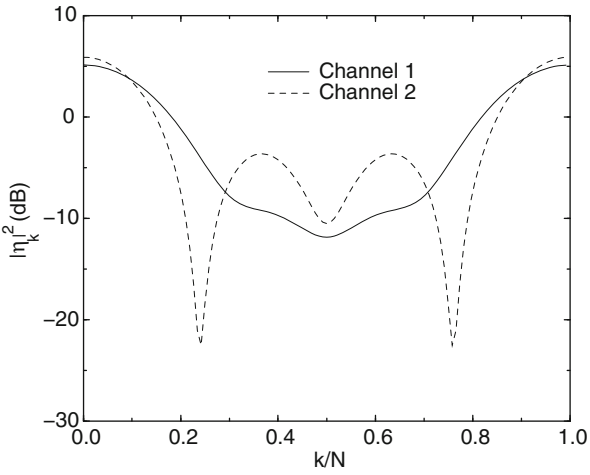

Fig. 10.3 Amplitude spectrum of static ISI channel with OFDM for $N = 128$

QAM Performance

The symbol error rate (SER) for 16-QAM is

$$\text{SER} = 3Q\left(\sqrt{\frac{1}{5}\gamma_s}\right)\left(1 - \frac{3}{4}Q\left(\sqrt{\frac{1}{5}\gamma_s}\right)\right), \tag{10.26}$$

where γ_s is the received symbol energy-to-noise ratio. With OFDM, the SER on static ISI channel is

$$\text{SER} = \frac{1}{N}\sum_{k=0}^{N-1}\text{SER}(k), \tag{10.27}$$

where $\text{SER}(k)$ is obtained from (10.26) with γ_s replaced by $\text{SIR}(k)$ from (10.20).

Two static ISI channels are considered as shown in Table 10.1. Channel 1 has sub-channels with a moderate null, whereas Channel 2 has several sub-channels with a severe null, as shown in Fig. 10.3.

Figure 10.4 shows the SER floors due to ISI without noise for different block sizes when a guard interval is not used $(G = 0)$. As expected, the error floor due to the ISI decreases with the increasing block size. However, when there exists deep

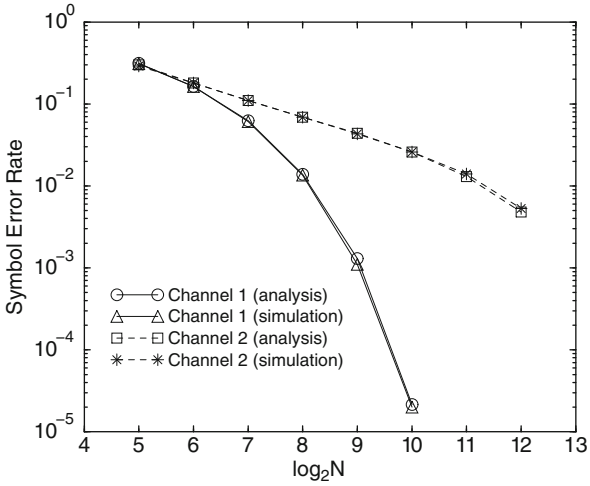

Fig. 10.4 Performance of OFDM signaling on static ISI channels with different block sizes; $G = 0$

null sub-channels as in Channel 2, the improvement from increasing block size is quite small. Therefore, increasing the OFDM block size is not always a very efficient countermeasure against ISI.

10.1.1.2 Fading ISI Channel

On fading ISI channels, channel time variations during a block causes ICI. For large block sizes, the central limit theorem can be invoked and the ICI can be treated like AWGN as shown in Sect. 5.7.1. If we assume 2D isotropic scattering and Rayleigh fading, then for large N the SIR is

$$\mathrm{SIR} = \frac{E_u}{E_s - E_u}, \tag{10.28}$$

where E_u is

$$E_u = \frac{E_s}{N^2}\left(\sum_{i=0}^{G}\mathrm{E}|g_i|^2\left(N + 2\sum_{m=1}^{N-1}(N-m)J_0(2\pi f_{\mathrm{m}}T_s m)\right)\right.$$
$$\left. + \sum_{i=G+1}^{L}\mathrm{E}|g_i|^2\left(N - i + G + 2\sum_{m=1}^{N-i-1+G}(N-i-m+G)J_0(2\pi f_{\mathrm{m}}T_s m)\right)\right). \tag{10.29}$$

The SER for a Rayleigh fading channel is obtained by averaging (10.26) over the probability density function

$$p_{\gamma_s}(x) = \frac{1}{\bar{\gamma}_s} e^{-\gamma_s/\bar{\gamma}_s}, \quad x \geq 0, \tag{10.30}$$

where $\bar{\gamma}_s$ is replaced by the SIR. The SER obtained using the SIR in (10.28) is actually an upper bound when the interference caused by ISI is a dominant factor. This is due to the correlation between the useful signal and interference term. An intuitive explanation is as follows. If the channel varies slowly, then we can assume the channel impulse response is constant over a duration of a block. Hence, from (10.20), the conditional SIR for the sub-channel k, given the channel impulse response $\mathbf{g} = \{g_m\}_{m=0}^{L}$, $\mathrm{SIR}(k|\mathbf{g})$, is

$$\mathrm{SIR}(k|\mathbf{g}) = \frac{\mathrm{E}[|\eta_k x_{\mathrm{n},k}|^2|\mathbf{g}]}{\mathrm{E}[|I_k|^2|\mathbf{g}]}. \tag{10.31}$$

For $L - G \ll N$ $\mathrm{SIR}(k|\mathbf{g})$ is well approximated by

$$\begin{aligned}\mathrm{SIR}(k|\mathbf{g}) = \frac{E_s}{2}\Bigg(&\frac{\sum_{i=0}^{G}\sum_{i'=0}^{G} g_i g_{i'}^* \exp\left\{-\mathrm{j}\frac{2\pi k}{N}(i-i')\right\}}{E_{\mathrm{ISI}}(k|\mathbf{g})} \\ &+ \frac{\sum_{i=0}^{G}\sum_{i'=G+1}^{L} g_i g_{i'}^* \exp\left\{-\mathrm{j}\frac{2\pi k}{N}(i-i')\right\}}{E_{\mathrm{ISI}}(k|\mathbf{g})} \\ &+ \frac{\sum_{i=G+1}^{L}\sum_{i'=G+1}^{L} g_i g_{i'}^* \exp\left\{-\mathrm{j}\frac{2\pi k}{N}(i-i')\right\}}{E_{\mathrm{ISI}}(k|\mathbf{g})}\Bigg),\end{aligned} \tag{10.32}$$

where $E_{\mathrm{ISI}}(k|\mathbf{g})$ is from (10.24) but expressed differently as

$$E_{\mathrm{ISI}}(k|\mathbf{g}) = \frac{E_s}{N}\sum_{i=G+1}^{L}\sum_{i'=G+1}^{L} g_i g_{i'}^* \min[i-G, i'-G] \exp\left\{-\mathrm{j}\frac{2\pi k(i-i')}{N}\right\}. \tag{10.33}$$

In (10.32), the first and second fractions represent the portion of SIR for which the Rayleigh assumption is valid in computing the SER, because the useful signal term and the interference term are uncorrelated. However, the last fraction shows that the useful signal term and the interference term are correlated. Hence, when the useful signal term is faded, so is the interference. Consequently, the Rayleigh assumption leads to pessimistic performance estimates, that is, the use of (10.28) to compute the SER gives an upper bound. On the other hand, if the portion of the energy contained within the guard interval is relatively large, then the last fraction becomes insignificant relative to the first two fractions in (10.32) and, hence, the SER found using the SIR from (10.28) is accurate.

Figure 10.5 shows the performance on a fading ISI channel that is based on the COST207 6-tap reduced typical urban channel model (see Sect. 2.5.4.1). Similar

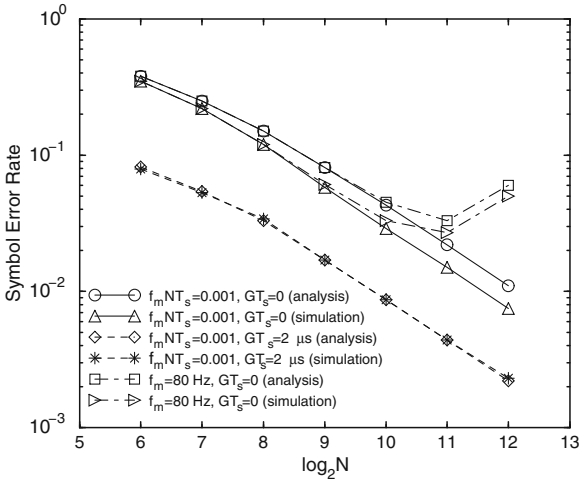

Fig. 10.5 Performance of OFDM signaling on fading ISI channels with different block sizes

to the case of static ISI channels, the performance improves as the block size is increased if the normalized Doppler frequency, $f_{\mathrm{m}}NT_{\mathrm{s}}$, is small. Unlike the static ISI channels, however, the block size cannot be made too large since this increases the ICI caused by channel time variations over block (Fig. 10.5). Therefore, the block size must be small enough to keep the ICI small, while it must be large enough to keep the ISI small for channels with a long impulse response. Also, as explained above, the SER from the analysis when $GT_{\mathrm{s}} = 2\ \mu$s agrees very well with simulation result but gives an upper bound when $G = 0$.

10.1.2 Residual ISI Cancelation

If the channel changes little during the block duration and the guard interval is sufficiently large, that is, $G \geq L$, then the channel output is

$$\tilde{R}_{n,m} = \sum_{i=0}^{L} g_i X_{n,(m-i)_N}, \quad 0 \leq m \leq N-1, \tag{10.34}$$

where $\tilde{R}_{n,m}$ represents the *desired* channel output that is free of ISI. However, when $G < L$ there will be residual ISI. To achieve the *desired* channel output $\tilde{R}_{n,m}$ in the presence of residual ISI, two steps must be followed. The first is to remove the residual ISI from the received signal, and the second is use reconstruction to restore cyclicity and avoid ICI. These two procedures are called *tail cancelation* and *cyclic reconstruction*, respectively [56]. The procedure can be described by

$$\tilde{R}_{n,m} = R_{n,m} - R_{n|n-1,m} + \sum_{i=G+1}^{L} g_i X_{n,(m-i)_N}(1 - u(m-i+G)). \tag{10.35}$$

The residual ISI is removed from the received signal by subtracting the second term in (10.35). Cyclicity is restored by the last term in (10.35).

The feasibility of implementing the tail cancelation and cyclic reconstruction procedures depends on the availability of the transmitted sample sequence $\{\mathbf{X}_n\}$ at the receiver. Echo cancelers have exact knowledge of the transmitted symbols and, therefore, the above procedures have been successfully implemented [56]. However, the vast majority of communication applications that require mitigation of ISI do not enjoy this luxury. We now describe the method for reducing the effect of ISI using aforementioned procedures when the transmitted symbols are not available to the receiver a priori.

10.1.2.1 Residual ISI Cancelation Algorithm

We assume that the channel impulse response is constant over a block period, that is, $g_{n,k} = g_n,\ 0 \le k \le N+G-1$. The RISIC algorithm proceeds as follows:

1. An estimate of the channel impulse response, $\hat{g}_n$, is obtained from a training sequence and updated in a decision-directed mode. Channel estimation will be treated in more detail in Sect. 10.1.3.3.
2. Decisions on the transmitted data symbols $\{\hat{x}_{n-1,k}\}$ from block $n-1$ are obtained for use in tail cancelation. Since the decisions are affected by residual ISI, some may be erroneous. These symbols are converted back to time-domain using an IDFT giving $\{\hat{X}_{n-1,m}\}$.
3. For the block of index n, we perform *tail cancelation* by calculating the residual ISI and subtracting it from $R_{n,m}$, that is,

$$\tilde{R}^{(0)}_{n,m} = R_{n,m} - \sum_{i=G+1}^{\hat{L}} \hat{g}_i \hat{X}_{n-1,(m-i)_N}(1-u(m-i+G)) \quad 0 \le m \le N-1 \quad (10.36)$$

   where $\hat{L}$ is the estimate of the maximum channel impulse response length.
4. The $\{\tilde{R}^{(0)}_{n,m}\}$ obtained in Step 3 are converted to the frequency-domain and decisions are made. Afterwards, the decisions are converted back to time-domain to give $\{\hat{X}^{(0)}_{n,m}\}$.
5. Next we perform *cyclic reconstruction* by forming

$$\tilde{R}^{(I)}_{n,m} = \tilde{R}^{(0)}_{n,m} + \sum_{i=G+1}^{\hat{L}} \hat{g}_i \hat{X}^{(I-1)}_{n,(m-i)_N}(1-u(m-i+G)), \quad 0 \le m \le N-1, \quad (10.37)$$

   where I represents an iteration number with an initial value of $I = 1$.
6. The $\{\tilde{R}^{(I)}_{n,m}\}$ are converted to the frequency-domain and decisions are made yielding $\{\hat{x}^{(I)}_{n,k}\}$. This completes the Ith iteration in the RISIC algorithm.

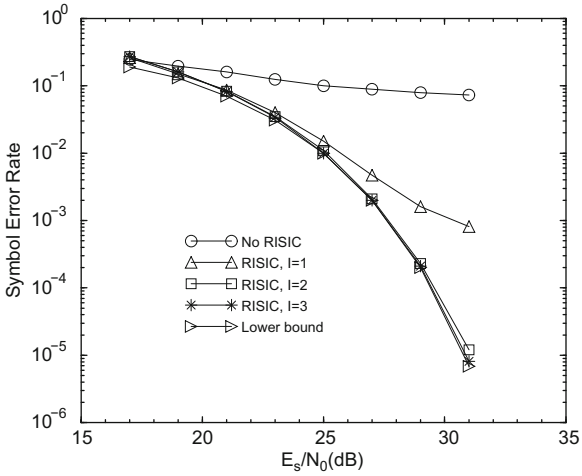

Fig. 10.6 Performance of the RISIC technique on channel 1; $G = 0, N = 128$

7. To continue iterations, convert the $\{\hat{x}_{n,k}^{(I)}\}$ to $\{\hat{X}_{n,m}^{(I)}\}$ and repeat Steps 5–7 with $I \leftarrow I + 1$.
8. End of the RISIC algorithm for block n.

10.1.3 Performance of the RISIC Algorithm

We now evaluate the performance of the RISIC algorithm on both static and fading ISI channels. The stability of the RISIC algorithm and the effect of using imperfect estimates of the channel impulse response is also investigated. Here we assume that $\hat{L} = L$, and note that choosing $\hat{L} > L$, for example, $\hat{L} = 2L$, will cause only a small degradation in performance.

10.1.3.1 Static ISI Channel

Suppose that the receiver has perfect channel information. The two static ISI channels in Table 10.1 are considered. Figures 10.6 and 10.7 illustrate the performance of the RISIC for Channels 1 and 2, respectively. RISIC offers a huge improvement in SER even after the first iteration, especially at high SNR. Several orders of magnitude improvement in SER are achievable for both channels after 2 or 3 iterations. The lower bounds shown in these figures are obtained by computing the SER using (10.27) without ISI and with noise only. On Channel 1, 2 iterations are required to effectively achieve the lower bound, while 3 iterations are required on Channel 2.

A periodic pilot sequence is needed even if perfect channel information is available, to prevent instability when feeding back a highly erroneous signal in the

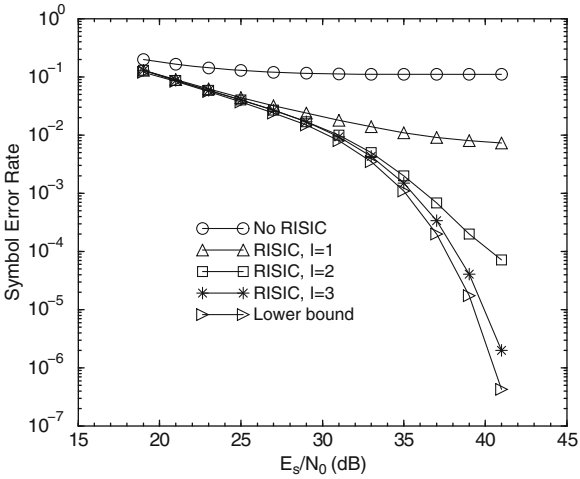

Fig. 10.7 Performance of the RISIC technique on channel 2; $G = 0, N = 128$

Table 10.2 Effect of using pilot sequence with RISIC technique

Overhead (%)	Without RISIC	SER ($I = 1$)	SER ($I = 2$)	SER ($I = 3$)
0	0.17	0.84	0.84	0.85
2	0.17	7.5×10^{-3}	2.9×10^{-4}	5.8×10^{-5}
5	0.17	7.5×10^{-3}	2.6×10^{-4}	3.1×10^{-5}

tail cancelation procedure. Table 10.2 shows the performance of RISIC on Channel 1 in Table 10.1 with $N = 64$ for $E_s/N_0 = 35\,\text{dB}$ and various training sequence overheads. Even with small overhead (2%), the SER improves dramatically, whereas the algorithm diverges when a pilot sequence is not used. Furthermore, only small degradation was observed with 2% overhead as compared to 5% overhead. If the block size is increased to $N = 128$, the RISIC algorithm converged for Channel 1 even when a pilot sequence was not used. Since many communications systems do utilize periodic training sequences for the purpose of synchronization or channel estimation, the need for additional overhead to maintain stability when applying RISIC may be unnecessary.

10.1.3.2 Fading ISI Channel

For fading ISI channels, the channel impulse response varies with time. However, if the channel changes little over a block duration and $L - G << N$, then

$$\{g_m\} \approx \frac{1}{\sqrt{N}} \text{IDFT}\{\eta_k\}. \tag{10.38}$$

When the channel variations are rapid, Fig. 10.5 shows that the performance is dominated by ICI rather than residual ISI. Assume η_k is known at the receiver

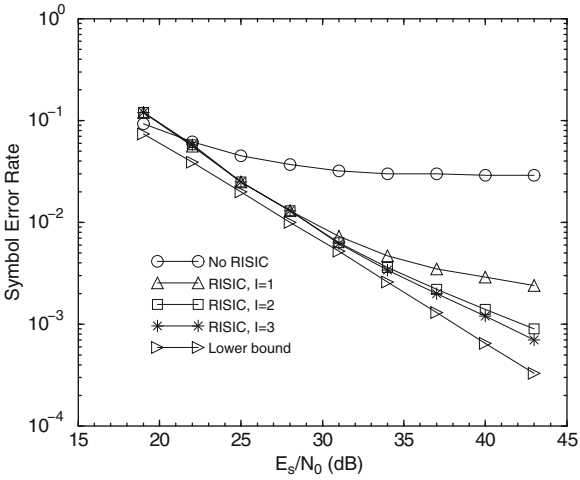

Fig. 10.8 Performance of the RISIC technique on a fading ISI channel; $G = 0$, $N = 1{,}024$, $f_{\mathrm{m}}NT_{\mathrm{s}} = 0.001$

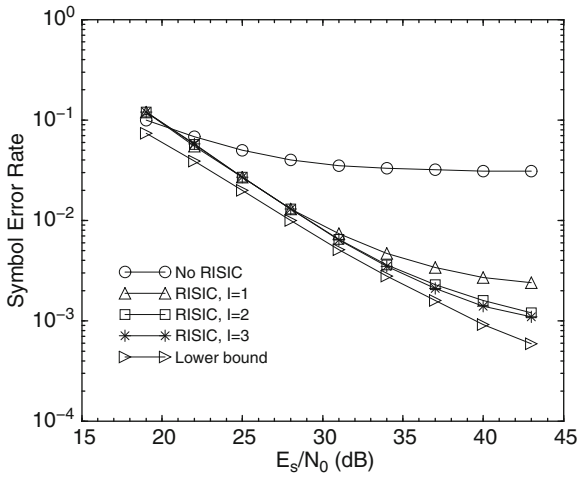

Fig. 10.9 Performance of the RISIC technique on a fading ISI channel; $G = 0$, $N = 1{,}024$, $f_{\mathrm{m}}NT_{\mathrm{s}} = 0.005$

and the channel impulse response is found by (10.38). Figures 10.8 and 10.9 show the performance of RISIC on a typical urban channel with $f_{\mathrm{m}}NT_{\mathrm{s}} = 0.001$ and $f_{\mathrm{m}}NT_{\mathrm{s}} = 0.005$, respectively, and 5% training overhead.

10.1.3.3 Channel Estimation

All the remarkable improvements that RISIC has shown so far are achieved under the premise of perfect channel information. For a strictly static ISI channel, the channel estimation process needs to be carried out only once. In fact, almost perfect channel estimates can be obtained using a training sequence [56]. Time-varying channels present the real challenge for channel estimation.

For fading ISI channels, we propose a channel estimation technique that can provide accurate estimates even in the presence of residual ISI. An OFDM training block can be used consisting of $N/2$ symbols chosen from a chirp sequence [56]

$$c_k = \exp\left\{\mathrm{j}\frac{2\pi}{N}k^2\right\},\ \ 0 \le k \le \frac{N}{2} - 1. \tag{10.39}$$

The chirp sequence provides an optimal PAPR of 1 and weighs each sub-channel equally in estimating the channel since the DFT of a chirp sequence is also chirp sequence. Unlike [56], however, we modify the training sequence to increase resilience to residual ISI, by inserting zeros in every odd sub-channel. The training block symbols are

$$d_k = \begin{cases} \sqrt{2}c_{k/2}, & k = 0, 2, \ldots, N-2, \\ 0, & k = 1, 3, \ldots, N-1, \end{cases} \tag{10.40}$$

where $\sqrt{2}$ is a normalization factor. The N-point IDFT of $\{d_k\}$ is[2]

$$D_m = C_{(m)_{N/2}},\ \ 0 \le m \le N-1. \tag{10.41}$$

From (10.41), the first half of the time-domain training sequence $\{D_m\}$ is identical to the second half. This is a valuable property for long channel impulse responses, because the first half of $\{D_m\}$ can be used just like a guard interval while $\{D_m\}$ still possesses a PAPR of 1. The channel estimation procedure using the proposed training block is as follows:

1. After removal of the guard interval, the received samples are re-arranged as

$$\bar{R}_{ts,m} = R_{ts,m+N/2},\ \ 0 \le m \le N/2 - 1, \tag{10.42}$$

   where the subscript ts indicates that the received samples are for a training block.
2. $N/2$ channel estimates, $\tilde{\eta}_k$, are calculated by

$$\tilde{\eta}_k = \frac{z_{ts,k}}{c_k},\ \ 0 \le k \le N/2 - 1, \tag{10.43}$$

   where $\{z_{ts,k}\}$ is the $N/2$-point DFT of $\{\bar{R}_{ts,m}\}$.
3. The estimates $\tilde{\eta}_k$ are converted to $\tilde{g}_m$ by

$$\{\tilde{g}_m\} = \frac{1}{\sqrt{N/2}}\mathrm{IDFT}\{\tilde{\eta}_k\}, \tag{10.44}$$

[2]The C_n can also be obtained by the $N/2$-point IDFT of $\{c_k\}$.

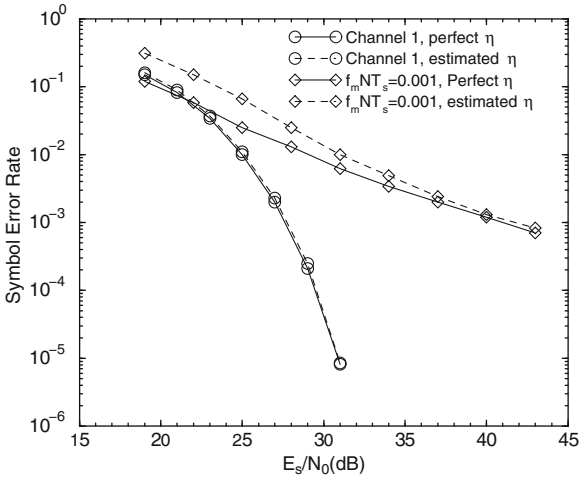

Fig. 10.10 Effect of imperfect channel estimation with the RISIC technique for static and slowly fading ISI channels with $N = 128$ and $N = 1{,}024$, respectively; $G = 0$, $I = 3$

where an $N/2$-point IDFT is used. Then, $\{\tilde{g}_m\}$ is passed through a rectangular window to zero $\tilde{g}_m$, $m > \hat{L}$, and the result is $\{\hat{g}_m\}$ which is used for RISIC.

4. $\{\hat{g}_m\}$ is converted to $\{\hat{\eta}_k\}$ by

$$\hat{\eta}_k = \sqrt{N}\,\mathrm{DFT}\{\hat{g}_m\}, \tag{10.45}$$

where this time an N-point DFT is used. The channel estimates for all N subchannels are now available for data demodulation.

When L is not known, the window size must be large enough to include the entire channel impulse response yet as small as possible to minimize the effect of noise.

On static ISI channels, the channel estimation is performed only once at the beginning of each simulation run and the channel estimates are averaged over four blocks. On fading ISI channels, the channel estimation is performed by periodically sending one training block out of every 20 blocks transmitted, while updating the channel estimate in the remaining blocks in a decision-directed mode [177]. In the decision directed mode, the decisions made after final iteration of the RISIC algorithm are used to update the channel estimates. Decision errors do not degrade the accuracy of the estimates excessively, because the rectangular window can smooth out the aberrations caused by the decision errors.

Figure 10.10 shows the performance of RISIC technique with channel estimation on static and very slowly fading ISI channels. For a static ISI channel, the SER obtained is virtually identical to that obtained with perfect channel estimation. For a slowly varying fading ISI channel ($f_{\mathrm{m}}NT_{\mathrm{s}} = 0.001$), the RISIC technique works well with the channel estimation, especially at high SNR. However, for faster fading ($f_{\mathrm{m}}NT_{\mathrm{s}} = 0.005$), the degradation is severe as shown in Fig. 10.11. This suggests that the proposed RISIC technique with channel estimation is well suited for static and slowly time-varying ISI channels.

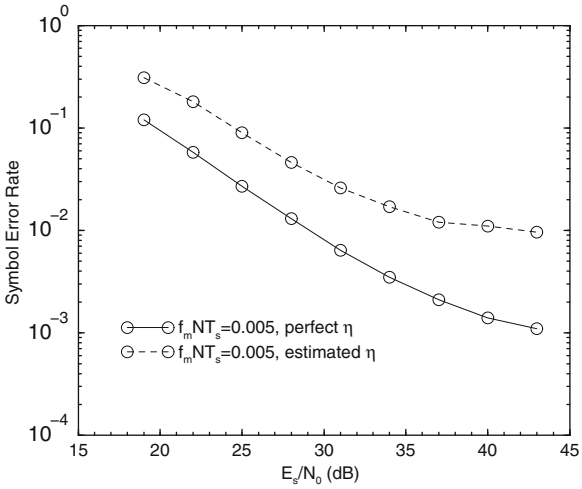

Fig. 10.11 Effect of imperfect channel estimation with the RISIC technique for a fading ISI channel; $N = 1{,}024$, $G = 0$, $I = 3$

10.2 Single-Carrier Frequency-Domain Equalization

As discussed in Sect. 10.1, OFDM can easily mitigate ISI using a cyclic guard interval. However, one of the major drawbacks of OFDM is its high PAPR and high sensitivity to oscillator frequency offsets. An attractive alternative to OFDM is the use of single-carrier (SC) modulation combined with FDE, simply known as SC-FDE [95, 230–232]. Such a system has the benefit of having the PAPR of single-carrier modulation while at the same time the ease of equalization of OFDM. For channels that span 10–20 data symbols, single-carrier systems with conventional time-domain equalization will have a significantly higher processing complexity than comparable OFDM approaches. However, the complexity of single-carrier approaches becomes similar to OFDM if FDE is used in the single-carrier receiver.

A typical SC-FDE transmitter is shown in Fig. 10.12, while the receiver is shown in Fig 10.13. In contrast to OFDM that uses an IDFT at the transmitter and a DFT at the receiver, an SC-FDE system has both the DFT and IDFT at the receiver side. SC-FDE can be used advantageously in wireless systems, using OFDM on the downlink and SC modulation on the uplink. With this arrangement, the mobile terminal transmits using SC modulation and, thus, it is simple to implement and can use a more efficient power amplifier. Also, the signal processing complexity is concentrated in the access point. For such full duplex operation, the access point has two IDFT and one DFT operations, while the mobile terminal has just one DFT operation.

One important difference between OFDM and SC-FDE is the exploitation of frequency diversity. OFDM can achieve maximum likelihood (ML) performance on a frequency selective channel through maximal ratio combining (MRC) of the symbols that are transmitted on the various sub-carriers. SC-FDE approaches are sub-optimal in this regard and do not achieve ML performance. Nevertheless,

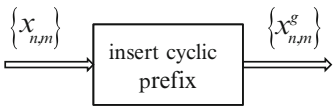

Fig. 10.12 SC-FDE transmitter with guard interval insertion

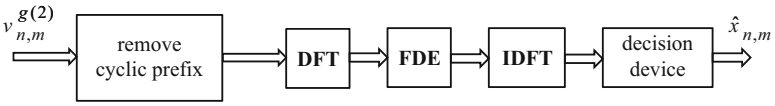

Fig. 10.13 SC-FDE receiver

OFDM only reaps the full benefits of frequency diversity by coding across the sub-carriers or using receiver antenna diversity. Uncoded OFDM will lose the inherent frequency diversity in the channel, since information data on the sub-carriers affected by the frequency-selective fading cannot be recovered from the other sub-carriers. On the other hand, the energy of each SC symbol is spread over complete frequency band, providing inherent frequency diversity. Due to higher frequency exploitation, uncoded SC-FDE outperforms uncoded OFDM . However, for a single-user, multi-antenna system (receive diversity) the advantage of SC-FDE over OFDM decreases as the number of receiver antennas increases.

Similar to the guard interval used in OFDM, with SC-FDE schemes a length-G cyclic guard interval is appended to each block of N data symbols, such that G equals or exceeds the maximum expected discrete-time channel length L. Here we assume a cyclic prefix. The cyclic prefix is added to the sequence $\mathbf{x}_n = \{x_{\mathrm{n},k},\ k = 0,\ldots N-1\}$ by simply copying the last G symbols of $\{x_{\mathrm{n},k}\}$ and appending them to the beginning of $\{x_{\mathrm{n},k}\}$. The symbol sequence with guard interval, denoted as $\{x^g_{n,k}\}$, is

$$\mathbf{x}^g_n = \{x_{\mathrm{n},(k)_N},\ \ k = -G, -G+1, \cdots, -1, 0, 1, \cdots, N-1\}, \tag{10.46}$$

where $(k)_N$ is the residue of k modulo-N. The sequence of $N+G$ symbols is then transmitted using SC modulation. Here, we assume a linear modulation scheme such as PSK or QAM, although SC-FDE can be applied with appropriate modification to nonlinear CPM as well [248]. With this assumption, the transmitted SC waveform has the form

$$\tilde{s}(t) = A\sum_n b(t - nT, \mathbf{x}^g_n), \tag{10.47}$$

where

$$b(t, \mathbf{x}^g_n) = \sum_{k=-G}^{N-1} x^g_{\mathrm{n},k} h_{\mathrm{a}}(t - kT^g_{\mathrm{s}}), \tag{10.48}$$

and $T = (N+G)T^g_{\mathrm{s}}$ is the duration of each data block consisting of N data symbols and G guard symbols.

10.2.1 ZF and MMSE SC-FDE

Suppose that the waveform $\tilde{s}(t)$ is transmitted over a time-invariant ISI channel with impulse response $g(t)$. We have established in Sect. 7.6.4 that the optimal front-end processing may be implemented as a filter that is matched to the transmitted pulse $h_{\rm a}(t)$ followed by rate-$2/T$ sampling and a $T/2$-spaced noise whitening filter $1/\left(G_h^{(2)}(1/z^*)\right)^*$. Similar to the development leading to (10.4), the received sample sequence at the output of the $T/2$-spaced whitened matched filter is

$$v_{n,k}^{g(2)} = \begin{cases} \sum\limits_{i=0}^{k+2G} g_{{\rm eq},i}^{(2)} x_{{\rm n},k-i}^{g(2)} + \sum\limits_{i=k+2G+1}^{2L} g_{{\rm eq},i}^{(2)} x_{{\rm n}-1,2N+2G+k-i}^{g(2)} + \tilde{w}_{n,k}^{(2)}, \\ \qquad\qquad -2G \le k < 2(-G+L), \\ \sum\limits_{i=0}^{2L} g_{{\rm eq},i}^{(2)} x_{{\rm n},k-i}^{g(2)} + \tilde{w}_{n,k}^{(2)}, \qquad 2(-G+L) \le k \le 2N-1, \end{cases} \tag{10.49}$$

where the sequence $\mathbf{x}_n^{g(2)} = \{x_{n,k}^{g(2)}\}$ is the corresponding $T/2$-spaced input symbol sequence given by

$$x_{n,k}^{g(2)} = \begin{cases} x_{k/2}^{g}, & k = -2G, \ldots, 0, 2, 4, \ldots, 2N-2 \\ 0, & k = -2G+1 \ldots, 1, 3, 5, \ldots, 2N-1 \end{cases} \tag{10.50}$$

and $\{g_{{\rm eq},i}^{(2)}\}$ is the $T/2$-spaced discrete-time channel impulse response with system function $G_{\rm eq}^{(2)}(z) = G_h^{(2)}(z)G^{(2)}(z)$.

The SC-FDE first removes the guard interval by simply deleting the first $2G$ samples in each block, that is, samples in the range $-2G \le k \le -1$. Under the assumption that $G \ge L$, this yields the length-$2N$ sequence

$$v_{n,k}^{(2)} = \sum_{i=0}^{2L} g_{{\rm eq},i}^{(2)} x_{{\rm n},k-i}^{g(2)} + \tilde{w}_{n,k}^{(2)} \tag{10.51}$$

$$= \sum_{i=0}^{2L} g_{{\rm eq},i}^{(2)} x_{{\rm n},(k-i)_N}^{(2)} + \tilde{w}_{n,k}^{(2)}, \quad 0 \le k \le 2N-1, \tag{10.52}$$

where

$$x_{n,k}^{(2)} = \begin{cases} x_{k/2}, & k = 0, 2, 4, \ldots, 2N-2, \\ 0, & k = 1, 3, 5, \ldots, 2N-1. \end{cases} \tag{10.53}$$

Note that the length-$2N$ vector $\mathbf{v}_n^{(2)} = \{v_{n,k}^{(2)}\}$ in (10.52) is the circular convolution of the length-$2N$ data sequence $\mathbf{x}_n^{(2)} = \{x_{n,k}^{(2)}\}$ with the length-$2L$ channel vector $\mathbf{g}_{\rm eq}^{(2)} = \{g_{{\rm eq},i}^{(2)}\}$.

To perform FDE, the length-$2N$ vector $\mathbf{v}_n^{(2)}$ is applied to a $2N$-point DFT or fast Fourier transform (FFT) to yield the output vector

$$\begin{aligned} V_{n,m}^{(2)} &= \frac{1}{2N}\sum_{k=0}^{2N-1} v_{n,k}^{(2)} \mathrm{e}^{-\mathrm{j}\frac{2\pi km}{2N}} \\ &= T_{\mathrm{eq},m}^{(2)} X_{n,m}^{(2)} + W_{n,m}^{(2)}, \ \ 0 \le m \le 2N-1, \end{aligned} \tag{10.54}$$

where

$$X_{n,m}^{(2)} = \frac{1}{2N}\sum_{k=0}^{2N-1} x_{n,k}^{(2)} \mathrm{e}^{-\mathrm{j}\frac{2\pi km}{2N}}, \ \ m = 0,\ldots,2N-1 \tag{10.55}$$

is the $2N$-point DFT of the data symbol vector $\mathbf{x}_n^{(2)}$,

$$T_{\mathrm{eq},m}^{(2)} = \sum_{k=0}^{L} g_{\mathrm{eq},m}^{(2)} \mathrm{e}^{-\mathrm{j}\frac{2\pi km}{N}}, \ \ m = 0,\ldots,2N-1 \tag{10.56}$$

is the channel frequency response, and the noise samples $\{W_{n,m}^{(2)}\}$ are i.i.d complex Gaussian random variables with zero-mean and variance $N_0/(2NT_{\mathrm{s}}^g)$. Note that $\mathbf{T}_{\mathrm{eq}}^{(2)} = \{T_{\mathrm{eq},m}^{(2)}\}_{m=0}^{2N-1}$ is the DFT of the zero-padded sequence $\mathbf{g}_{\mathrm{eq}}^{(2)} = \{g_{\mathrm{eq},k}^{(2)}\}_{k=0}^{N-1}$ and is equal to the sampled frequency response of the channel. Also, since every other coordinate of the vector $\mathbf{x}_n^{(2)}$ is zero, we have the property $X_{n,m}^{(2)} = X_{n,m+N}^{(2)}$ for $m = 0,\ldots,N-1$, that is, the first half of the length-$2N$ vector $\mathbf{X}_n^{(2)} = \{X_{n,m}^{(2)}\}_{m=0}^{2N-1}$ is identical to the last half.

FDE may now be carried out by processing the vector $\mathbf{V}_n^{(2)} = \{V_{n,m}^{(2)}\}$. One option is to estimate $T_{\mathrm{eq},m}^{(2)}$ and calculate

$$\begin{aligned} \hat{V}_{n,m}^{(2)} &= \frac{V_{n,m}^{(2)}}{T_{\mathrm{eq},m}^{(2)}} \\ &= X_{n,m}^{(2)} + \frac{W_{n,m}^{(2)}}{T_{\mathrm{eq},m}^{(2)}}, \ \ m = 0,\ldots,2N-1. \end{aligned} \tag{10.57}$$

This is sometimes called zero-forcing frequency-domain equalization (ZF-FDE), because we try to invert the channel in the frequency-domain. Afterwards, the $2N$-point IDFT of the vector $\hat{\mathbf{V}}_n^{(2)} = \{\hat{V}_{n,m}^{(2)}\}_{m=0}^{2N-1}$ is calculated to yield the length-$2N$ vector $\tilde{\mathbf{x}}_n^{(2)} = \{\tilde{x}_{n,k}^{(2)}\}$, where

$$\tilde{x}_{n,k}^{(2)} = x_{n,k}^{(2)} + \tilde{w}_{n,k}^{(2)}, \ \ k = 0,\ldots,2N-1 \tag{10.58}$$

and

$$\tilde{w}_{n,k}^{(2)} = \sum_{m=0}^{N-1} \left(\frac{W_{n,m}^{(2)}}{T_{\mathrm{eq},m}^{(2)}} \right) \mathrm{e}^{\frac{\mathrm{j}2\pi mk}{2N}}, \quad k = 0,\ 1,\ \ldots,\ 2N-1. \tag{10.59}$$

The length-$2N$ vector $\tilde{\mathbf{x}}_n^{(2)}$ is then decimated by taking every other sample, that is, $\tilde{x}_{n,k} = \tilde{x}_{n,2k}^{(2)},\ k = 0, \ldots, N-1$, and decisions are made from the resulting vector $\tilde{\mathbf{x}}_n = \{\tilde{x}_{n,k}\}$. For *each* of the $\tilde{x}_{n,k}$, the receiver decides in favor of the data symbol $x_{n,k}$ that minimizes the squared Euclidean distance

$$\mu(x_{\mathrm{n},k}) = \|\tilde{x}_{n,k} - x_{n,k}\|^2, \ \ k = 0, \ldots, N-1. \tag{10.60}$$

Observe that the noise samples $W_{n,m}^{(2)}/T_{\mathrm{eq},m}^{(2)}$ in (10.57) are independent zero-mean complex Gaussian random variables with variance $N_0/(2NT_{\mathrm{s}}^g|T_{\mathrm{eq},m}^{(2)}|^2))$. Hence, the noise is amplified in sub-bands where $|T_{\mathrm{eq},m}^{(2)}|$ is small, and if $|T_{\mathrm{eq},m}^{(2)}|$ is very small $\hat{V}_{n,m}^{(2)}$ will be corrupted by heavy noise. This effect is similar to noise enhancement in time-domain ZF linear equalizers and can severely degrade the bit error probability.

Another possibility is to account for the effects of noise enhancement by performing minimum mean square error frequency-domain equalization (MMSE-FDE). Assume that the MMSE-FDE has tap gains $C_m, m = 0, \ldots, N-1$. Then the output of the MMSE-FDE is

$$\begin{aligned} \hat{V}_{n,m}^{(2)} &= V_{n,m}^{(2)} C_m \\ &= T_{\mathrm{eq},m}^{(2)} X_{n,m}^{(2)} C_m + W_{n,m}^{(2)} C_m, \ \ 0 \le m \le 2N-1. \end{aligned} \tag{10.61}$$

The mean square error is defined as

$$\begin{aligned} J &= \frac{1}{2}\mathrm{E}\left[|\hat{V}_{n,m}^{(2)} - X_{n,m}^{(2)}|^2 \right] \\ &= |T_{\mathrm{eq},m}^{(2)} C_m - 1|^2 \sigma_x^2/(2N) + |C_m|^2 N_0/(2N) \\ &= \left(T_{\mathrm{eq},m}^{(2)} \sigma_x^2 + N_0 \right) |C_m|^2/(2N) - 2\hat{A}\sigma_x^2 \mathrm{Re}\left\{ T_{\mathrm{eq},m}^{(2)} C_m \right\}/(2N) + \sigma_x^2/(2N), \end{aligned} \tag{10.62}$$

where the second line uses $\frac{1}{2}\mathrm{E}[|X_{n,m}^{(2)}|^2] = \sigma_x^2/(2N)$ as seen from Parseval's theorem

$$\frac{1}{2N} \sum_{k=0}^{2N-1} |\tilde{x}_{n,k}^{(2)}|^2 = \sum_{m=0}^{2N-1} |X_{n,m}^{(2)}|^2. \tag{10.63}$$

The MMSE solution can be obtained by solving

$$\frac{\mathrm{d}J}{\mathrm{d}C_m} = \frac{\mathrm{d}J}{\mathrm{C}_{R,m}} + \mathrm{j}\frac{\mathrm{d}J}{\mathrm{d}C_{I,m}} = 0, \ \ m = 0, \ldots, N-1, \tag{10.64}$$

where $C_m = C_{R,m} + \mathrm{j}C_{I,m}$. This gives the solution

$$C_m = \frac{\sigma_x^2 T_{\mathrm{eq},m}^{(2)\,*}}{\sigma_x^2 |T_{\mathrm{eq},m}^{(2)}|^2 + N_0}, \quad m = 0, \ldots, 2N-1. \tag{10.65}$$

Note that under high signal-to-noise ratio conditions where $N_0 \to 0$, the tap solution for the MMSE-FDE in (10.65) reduces to the ZF-FDE tap solution $C_m = 1/T_{\mathrm{eq},m}^{(2)}$ used in (10.57). The output of the MMSE-FDE is

$$\begin{aligned} \hat{V}_{n,m}^{(2)} &= V_{n,m}^{(2)} C_m \\ &= \frac{\sigma_x^2 |T_{\mathrm{eq},m}^{(2)}|}{\sigma_x^2 |T_{\mathrm{eq},m}^{(2)}|^2 + N_0} X_{n,m}^{(2)} + \frac{\sigma_x^2 T_{\mathrm{eq},m}^{(2)\,*}}{\sigma_x^2 |T_{\mathrm{eq},m}^{(2)}|^2 + N_0} W_{n,m}^{(2)}, \quad m = 0, \ldots, 2N-1. \end{aligned} \tag{10.66}$$

Once again, the IDFT of the vector $\hat{\mathbf{V}}_n^{(2)} = \{\hat{V}_{n,m}^{(2)}\}_{i=0}^{2N-1}$ is obtained to yield the vector $\tilde{\mathbf{x}}_n^{(2)}$, which is then decimated to yield the vector $\tilde{\mathbf{x}}_n = \{\tilde{x}_{n,k} = \tilde{x}_{n,2k}^{(2)}, k = 0, \ldots, N-1\}$, and the vector $\tilde{\mathbf{x}}_n$ is applied to a minimum distance decision device as in (10.60).

Finally, we repeat that while decisions variables $\tilde{z}_{n,k}$ in (10.8) can be used to implement maximum likelihood decisions in an OFDM receiver, the corresponding decision variables $\tilde{x}_{n,k}$ in an SC-FDE receiver will *not* yield maximum likelihood decisions. In this sense, the SC-FDE approach is sub-optimal.

10.3 Orthogonal Frequency Division Multiple Access

OFDMA achieves multiple access by assigning different users disjoint sets of sub-carriers. Assume that there are a total of M sub-carriers that are evenly distributed among Q users, such that each user is allocated $N = M/Q$ sub-carriers. The overall sub-carriers are labeled with indices from 0 to $M-1$, while the N sub-carriers allocated to the jth MS have indices that belong to the set $\mathscr{T}_j$. Clearly, the sets $\mathscr{T}_j$ must be disjoint such that each sub-carrier is assigned to at most one MS. The sub-carrier allocation can be performed by extending the nth data vector for the jth MS, denoted, by $\mathbf{a}_{j,n}$ with the insertion of $M-N$ zeros in the sub-carriers belonging the set $\bar{\mathscr{T}}_j$ which is the complement of $\mathscr{T}_j$, that is,

$$x_{j,n,i} = \begin{cases} a_{j,n,i}, & \text{if } i \in \mathscr{T}_j, \\ 0, & \text{otherwise}, \end{cases} \tag{10.67}$$

where $a_{j,n,i}$ is the data symbol transmitted to the jth MS in block n on the ith sub-carrier.

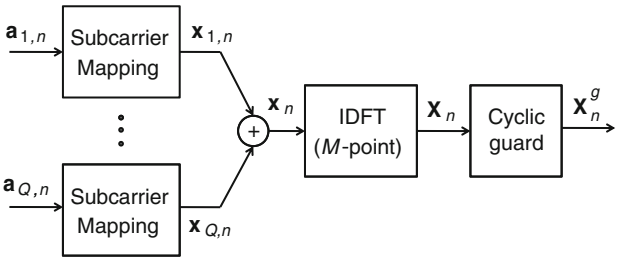

Fig. 10.14 Baseband OFDMA forward link BS transmitter. There are M sub-carriers of which N are occupied by the input data for each of Q users

10.3.1 OFDMA Forward Link

10.3.1.1 Transmitter

A block diagram of an OFDMA baseband forward link transmitter is shown in Fig. 10.14. On the forward link, the vectors $\mathbf{x}_{j,n} = \{x_{j,n,i}\}_{i=0}^{M-1}$ are summed up to produce the nth data block

$$\mathbf{x}_n = \sum_{j=1}^{Q} \mathbf{x}_{j,n} \tag{10.68}$$

that is subsequently applied to an M-point IDFT to produce the length-M time-domain sequence $\mathbf{X}_n$. After the IDFT, a length-G guard interval is appended to each block in the form of a cyclic prefix or cyclic suffix, in the same manner as conventional OFDM as described in Sect. 4.6.3, to yield the transmitted time-domain sequence $\mathbf{X}_n^g$. In the case of a cyclic prefix, the last G symbols of the sequence $\mathbf{X}_n = \{X_{n,m},\ m = 0,\ldots,M-1\}$ are copied and appended to the beginning of $\mathbf{X}_n$. The transmitted time-domain sequence for the nth block with a cyclic prefix, denoted as $\mathbf{X}_n^g$, is

$$\mathbf{X}_n^g = \{X_{n,(m)_M},\ m = -G, -G+1, \cdots, -1, 0, 1, \cdots, M-1\}, \tag{10.69}$$

where $(m)_M$ is the residue of m modulo-M.

10.3.1.2 Time-Domain Windowing

The elements of the vector $\mathbf{X}_n^g$ are converted into the continuous-time complex-valued waveform using pair of balanced DACs, as discussed in Sect. 4.6.3. The resulting continuous-time complex envelope corresponding to the nth block is

$$\tilde{s}_n(t) = \sum_{k=-G}^{M-1} X_{n,k}^g h_{\mathrm{DAC}}(t - k\tilde{T}_s^g), \tag{10.70}$$

where $h_{\mathrm{DAC}}(t)$ is the impulse response of the DAC (reconstruction filter) and $\tilde{T}_{\mathrm{s}}^{g}$ is the sample period. For OFDMA, the sample period is equal to $\tilde{T}_{\mathrm{s}}^{g} = (M/(M+G))\tilde{T}_{\mathrm{s}} = (N/(M+G))T_{\mathrm{s}}$ seconds.

For greater spectral control and to reduce out-of-band emissions, the vector of samples $\mathbf{X}_n^g$ can be windowed prior to digital-to-analog conversion, such that

$$\tilde{s}_n(t) = \sum_{k=-G}^{M-1} X_{n,k}^{g} w_k h_{\mathrm{DAC}}(t - k\tilde{T}_{\mathrm{s}}^{g}), \tag{10.71}$$

where the vector $\mathbf{w} = (w_{-G}, \ldots, w_{-1},\ w_0,\ w_1, \ldots, w_{M-1})$ is the window function. The corresponding continuous-time window function $w(t)$ can be obtained by passing the weighted impulse train

$$\delta_{\tilde{T}_{\mathrm{s}}^{g}}(t) = \sum_{k=-G}^{M-1} w_k \delta(t - k\tilde{T}_{\mathrm{s}}^{g}), \tag{10.72}$$

through the reconstruction filter $h_{\mathrm{DAC}}(t)$. Here, we assume an ideal DAC with impulse response

$$h_{\mathrm{DAC}}(t) = \mathrm{sinc}(t/\tilde{T}_{\mathrm{s}}^{g}). \tag{10.73}$$

For a rectangular window, $w_n = 1,\ -G \le n \le M-1$. This yields the continuous-time window function

$$w(t) = \sum_{k=-G}^{M-1} \mathrm{sinc}(t/\tilde{T}_{\mathrm{s}}^{g} - k), \tag{10.74}$$

which is plotted in Fig. 10.15 for the case $M = 32, G = 4$. Notice that the continuous-time window function $w(t)$ is noncausal, since the ideal DAC is itself a noncausal ideal low-pass filter.

With an ideal DAC, the power spectrum of the baseband OFDMA waveform is confined to $-1/2\tilde{T}_{\mathrm{s}}^{g}$ to $+1/2\tilde{T}_{\mathrm{s}}^{g}$ Hz. However, a practical DAC will produce side lobes outside of this range of frequencies and, in some cases, the rectangular window may result in large side lobes. Such out-of-band emissions can be reduced using a time-domain window that smooths the ends of the OFDMA symbols. Such windowing can be implemented by extending the OFDMA symbol with both a cyclic prefix and cyclic suffix as shown in Fig. 10.16. That is,

$$\mathbf{X}_n^g = \{X_{n,(m)_M},\ m = -G_{\mathrm{p}}, \cdots, -1, 0, 1, \cdots, M-1,\ , \ldots, M + G_{\mathrm{s}} - 1\}, \tag{10.75}$$

where G_{p} and G_{s} are the length of the cyclic prefix and cyclic suffix, respectively, and $G = G_{\mathrm{p}} + G_{\mathrm{s}}$ is the total length of the guard interval. In this way, the required extension to implement the time-domain window can absorbed into the guard interval. This will save in bandwidth and power efficiency but will also reduce the delay spread tolerance by $2G_{\mathrm{s}}$ samples.

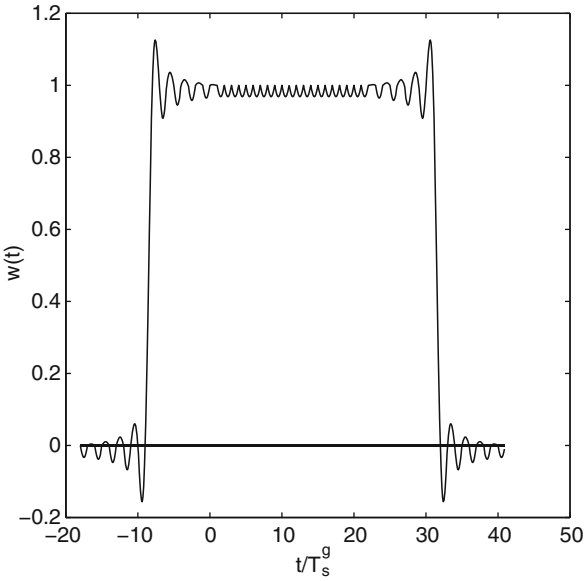

Fig. 10.15 Continuous-time rectangular window function $w(t)$, $M = 32$, $G = 8$

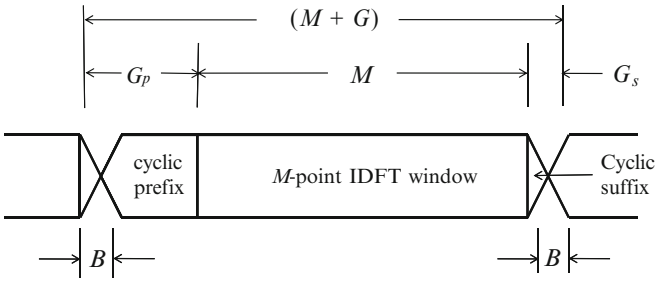

Fig. 10.16 OFDMA symbols with time-domain windowing. Note that $B = G_s + 1$, where G_s is the length of the cyclic suffix and B is the length of the transition region

One commonly used time-domain window function with OFDM/OFDMA is the raised cosine window

$$w_k^{\text{rc}} = \begin{cases} \frac{1}{2} + \frac{1}{2}\sin\left[\frac{\pi}{B}\left(k - \frac{B-1}{2}\right)\right], & 0 \le k < B, \\ 1, & B \le k < M+G-B, \\ \frac{1}{2} - \frac{1}{2}\sin\left[\frac{\pi}{B}\left(k - M - G + \frac{B+1}{2}\right)\right] & M+G-B \le k \le M+G-1, \\ 0, & \text{elsewhere}, \end{cases} \tag{10.76}$$

defined here on the interval $0 \le k \le M + G - 1$. For the sequence $\mathbf{X}_n^g$ in (10.75), the required window is the raised cosine window in (10.76) left shifted by G_p samples, such that

$$w_k = w_{k+G_p}^{\text{rc}}. \tag{10.77}$$

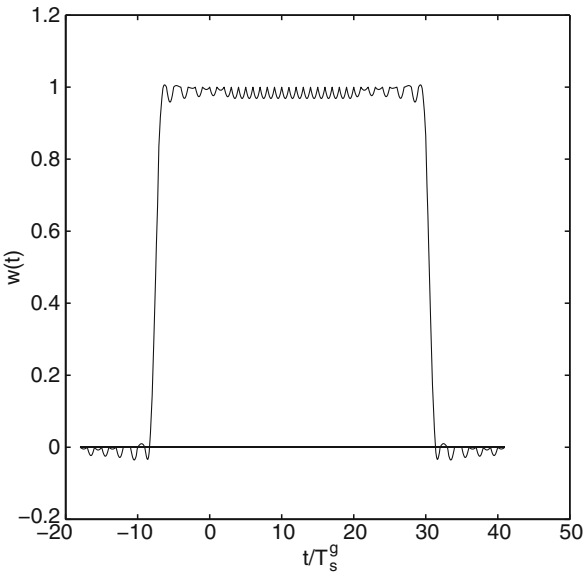

Fig. 10.17 Continuous-time raised cosine window function $w(t)$, $M = 32$, $G_\mathrm{p} = 4$, $G_\mathrm{s} = 4$

After passing through an ideal D/A converter, this will yield the continuous-time pulse

$$w(t) = \sum_{k=-G}^{M-1} w_k \mathrm{sinc}(t/\tilde{T}_\mathrm{s}^g - k), \tag{10.78}$$

which is plotted in Fig. 10.17 for the case $M = 32, G_\mathrm{p} = 4, G_\mathrm{s} = 4$. Notice that the raised cosine windowing has also significantly reduced the peaks on the amplitude shaping pulse. Hence, the time-domain windowing not only produces a more compact power spectral density, but it also reduces the PAPR of the transmitted waveform.

10.3.1.3 Sub-carrier Allocation

Several different methods for sub-carrier allocation are used with OFDMA. The choice of sub-carrier allocation will affect the sensitivity of the OFDMA waveform to frequency-selective fading.

Clustered Carrier (CC-OFDMA)

With CC-OFDMA, the M sub-carriers are divided into Q groups where each group consists of N contiguous sub-carriers called clusters. The set of sub-carrier indices allocated to the kth user is $\{kN, kN+1, \ldots, kN+N-1\}$, where $0 \leq k < Q$. CC-OFDMA is sensitive to frequency-selective fading, because all sub-carriers assigned to a particular user may fade simultaneously.

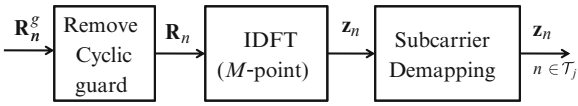

Fig. 10.18 Baseband OFDMA forward link receiver

Spaced Carrier (SC-OFDMA)

With SC-OFDMA, the M sub-carriers are partitioned into N groups, where each group has Q contiguous sub-carriers. Then the kth sub-carrier of each group is assigned to the kth user. That is, the kth user is assigned the set of sub-carrier indices $\{k, Q+k, \ldots, (N-1)Q+k\}$, where $0 \le k < Q$. SC-OFDMA is less sensitive to frequency-selective fading, since the sub-carriers assigned to each user span the entire bandwidth.

Random Interleaving (RI-OFDMA)

RI-OFDMA has been adopted by IEEE802.16a. While the sub-carriers are partitioned into N groups as in SC-OFDMA, the sub-carrier index in each of the N groups that is assigned to a particular user is a random variable. The sub-carrier indices allocated to the kth user are $\{\varepsilon_{k,1}, Q+\varepsilon_{k,2}, \ldots, (M-1)Q+\varepsilon_{k,M-1}\}$, where the $\varepsilon_{k,i}$ are independent and identically distributed uniform random variables on the set $\{0, 1, \ldots, Q-1\}$. However, each sub-carrier can be assigned to at most one user.

10.3.1.4 Receiver

Similar to the case of OFDM in Sect. 10.1, consider the transmission of the OFDMA waveform over a frequency-selective quasi-static fading channel. Assuming a length-G cyclic prefix, the discrete-time linear convolution of the transmitted sequence $\{\mathbf{X}_n^g\} = \{X_{n,m}\}_{m=-G}^{M-1}$ with the discrete-time channel impulse response $\mathbf{g} = \{g_m\}_{m=0}^{L}$ produces the discrete-time received sequence $\mathbf{R}_n^g = \{R_{n,m}^g\}$, where

$$R_{n,m}^g = \begin{cases} \sum_{i=0}^{m+G} g_i X_{n,m-i}^g + \sum_{i=m+G+1}^{L} g_i X_{n-1,M+G+m-i}^g + \tilde{n}_{n,m}, & -G \le m < -G+L, \\ \sum_{i=0}^{L} g_i X_{n,m-i}^g + \tilde{n}_{n,m}, & -G+L \le m \le M-1 \end{cases} \tag{10.79}$$

and the $\tilde{n}_{n,m}$ are complex-valued Gaussian noise samples having zero-mean and variance $\sigma^2 = \frac{1}{2}\mathrm{E}[|\tilde{n}_{n,m}|^2] = N_0/T_\mathrm{s}^g$, where $T_\mathrm{s}^g = NT_\mathrm{s}/(M+G)$, and T_s is the modulation symbol rate for each user.

The OFDMA baseband receiver is shown in Fig. 10.18. To remove the ISI introduced by the channel, the first G received samples $\{R_{n,m}^g\}_{m=-G}^{-1}$ of each block are simply discarded. If the length of the cyclic prefix is at least as long as the discrete-time channel length, that is, $G \ge L$, then we obtain the received sequence

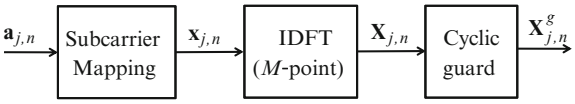

Fig. 10.19 Baseband OFDMA reverse link MS transmitter. There are M sub-carriers of which N are occupied by the input data

$$\begin{aligned} R_{n,m} &= R^{g}_{n,m} \\ &= \sum_{i=0}^{L} g_i X_{n,(m-i)_M} + \tilde{n}_{n,m}, \quad 0 \le m \le M-1, \end{aligned} \tag{10.80}$$

which is just the circular convolution of the transmitted sequence $\mathbf{X}_n = \{X_{n,m}\}$ with the channel $\mathbf{g} = \{g_m\}_{m=0}^{L}$. Afterwards, an M-point IDFT is taken to transform to the frequency-domain. This yields the output vector

$$\begin{aligned} z_{n,i} &= \frac{1}{M} \sum_{m=0}^{M-1} R_{n,m} \mathrm{e}^{-\mathrm{j}\frac{2\pi mi}{M}} \\ &= T_i A x_{\mathrm{n},i} + \nu_{n,i}, \quad 0 \le i \le M-1, \end{aligned} \tag{10.81}$$

where

$$T_i = \sum_{m=0}^{L} g_m \mathrm{e}^{-\mathrm{j}\frac{2\pi mi}{M}}, \tag{10.82}$$

and the noise samples $\{\nu_{n,i}\}$ are i.i.d with zero-mean and variance $N_0/(MT_{\mathrm{s}}^{g})$. On the forward link each MS will only be interested in the N data symbols that are transmitted by the BS on its allocated sub-carriers. Hence, only the DFT outputs with indices in the set $\mathscr{T}_j$ are used by the jth MS for data detection. The resulting time-domain sequence is further processed, using for example maximum likelihood sequence estimation (MLSE) along with the estimates of the channel gains $\{T_i\}, i \in \mathscr{T}_j$.

10.3.2 OFDMA Reverse Link

On the OFDMA reverse link, Q users transmit their signals to a central BS. The reverse link MS transmitter is shown in Fig. 10.19, and is similar to the forward link BS transmitter in Fig. 10.14. The main difference is that the MS transmitter only transmits its own data stream, whereas the BS transmitter sends data streams simultaneously for all the MSs. Similar to the OFDMA forward link, the jth MS performs sub-carrier allocation according to (10.67), and the resulting vector $\mathbf{x}_{j,n}$ is applied to an M-point IDFT, and appended with a length-G cyclic guard interval.

10.3.3 Peak-to-Average Power Ratio

One of the biggest drawbacks of OFDMA is its high PAPR. A high PAPR may be tolerable on the forward link, since the BS can use a less power efficient linear amplifier. However, for the reverse link, a high PAPR is undesirable since the MS is often battery powered. For this reason, OFDMA is not used on the reverse link of LTE and LTE-A.

10.4 Single-Carrier Frequency Division Multiple Access

A block diagram of an SC-FDMA transmitter is shown in Fig. 10.20. The SC-FDMA transmitter groups the modulation symbols into blocks of N symbols. Let

$$\mathbf{x}_n = (x_{\mathrm{n},1}, x_{\mathrm{n},2}, \ldots, x_{\mathrm{n},N}), \tag{10.83}$$

denote the nth block of modulation symbols. An N-point DFT (N-DFT) is taken on each block $\mathbf{x}_n$, to yield length-N vectors

$$\mathbf{X}_n = (X_{n,1}, X_{n,2}, \ldots, X_{n,N}), \tag{10.84}$$

that are the frequency-domain representation of the blocks of input symbols. The sub-carrier mapper then maps the N components of the vector $\mathbf{X}_n$ onto a larger set of M sub-carriers such that $M = NQ$, where Q is an integer. There are several different types of sub-carrier mappings, including the interleaved (I-FDMA) and localized (L-FDMA) mappings that are considered below. The sub-carrier mapping generates the sequence $\tilde{\mathbf{X}}_n$. An M-point IDFT is then taken of the sequence $\tilde{\mathbf{X}}_n$ to produce the output sequence $\tilde{\mathbf{x}}_n$. The time-domain input symbols $x_{\mathrm{n},k}$ have duration T_s seconds. However, after going through the SC-FDMA modulator the time-domain output symbols $\tilde{x}_{n,k}$ are compressed and have duration $\tilde{T}_\mathrm{s} = (N/M)T_\mathrm{s}$ seconds.

The SC-FDMA baseband receiver is shown in Fig. 10.21. First, the cyclic guard interval is removed. Afterwards, an M-point DFT is taken to transform to the frequency-domain. Sub-carrier demapping and equalization is then performed in the frequency-domain. Finally, an N-point IDFT is used to convert the samples back to the time-domain for detection and further processing.

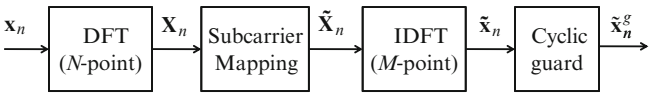

Fig. 10.20 Baseband SC-FDMA transmitter. There are M sub-carriers of which N are occupied by the input data

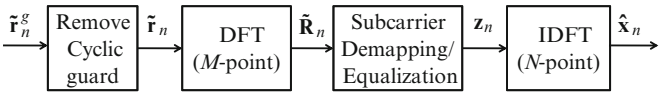

Fig. 10.21 Baseband SC-FDMA receiver with SC-FDE

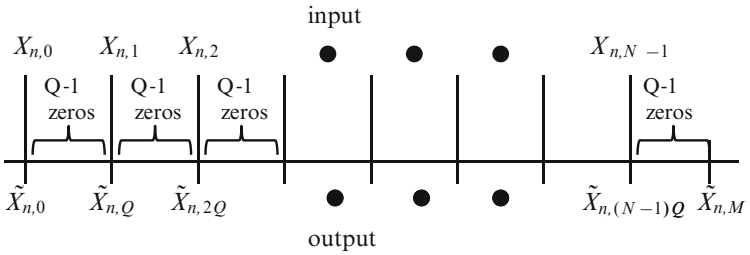

Fig. 10.22 Interleaved FDMA (I-FDMA) sub-carrier mapping

Interleaved (I-FDMA)

The I-FDMA sub-carrier mapping is illustrated in Fig. 10.22 and can be described as follows:

$$\tilde{X}_{n,\ell} = \begin{cases} X_{n,\ell/Q}, & \ell = kQ,\ \ 0 \le k \le N-1, \\ 0, & \text{otherwise.} \end{cases} \tag{10.85}$$

The time-domain vector $\tilde{\mathbf{x}}_n$ is obtained by taking the M-point inverse DFT of the vector $\tilde{\mathbf{X}}_n$. Let $k = Nq + m$, where $0 \le q \le Q-1$ and $0 \le m \le N-1$. Then

$$\begin{aligned} \tilde{x}_{n,k} \equiv \tilde{x}_{n,Nq+m} &= \frac{1}{M} \sum_{\ell=0}^{M-1} \tilde{X}_{n,\ell} \mathrm{e}^{\mathrm{j}\frac{2\pi\ell k}{M}} \\ &= \frac{1}{QN} \sum_{\ell=0}^{N-1} X_{n,\ell} \mathrm{e}^{\mathrm{j}\frac{2\pi\ell k}{N}} \\ &= \frac{1}{QN} \sum_{\ell=0}^{N-1} X_{n,\ell} \mathrm{e}^{\mathrm{j}\frac{2\pi\ell(Nq+m)}{N}} \\ &= \frac{1}{Q} \left(\frac{1}{N} \sum_{\ell=0}^{N-1} X_{n,\ell} \mathrm{e}^{\mathrm{j}\frac{2\pi\ell m}{N}} \right) \\ &= \frac{1}{Q} x_{\mathrm{n},m}. \end{aligned} \tag{10.86}$$

It follows that the time-domain vector $\tilde{\mathbf{x}}_n$ is equal to

$$\tilde{\mathbf{x}}_n = \frac{1}{Q} \mathrm{vec}(\mathbf{x}_n, \mathbf{x}_n, \ldots, \mathbf{x}_n), \tag{10.87}$$

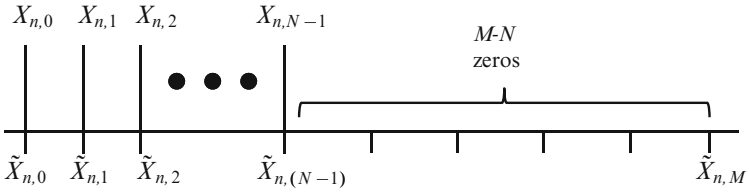

Fig. 10.23 Localized FDMA (L-FDMA) sub-carrier mapping

which is just the Q-fold repetition of the time-domain vector $\mathbf{x}_n$. It also follows that the PAPR of the time-domain sequence $\tilde{\mathbf{x}}_n$ is exactly the same as that of the time-domain sequence $\mathbf{x}_n$.

Localized (L-FDMA)

The L-FDMA, the sub-carrier mapping is illustrated in Fig. 10.23 and can be described as follows:

$$\tilde{X}_{n,\ell} = \begin{cases} X_{n,\ell}\,, & 0 \le \ell \le N-1, \\ 0\,, & N \le \ell \le M-1. \end{cases} \tag{10.88}$$

The time-domain vector $\tilde{\mathbf{x}}_n$ is obtained by taking the M-point inverse DFT of the vector $\tilde{\mathbf{X}}_n$. Let $k = Qm + q$, where $0 \le m \le N-1$ and $0 \le q \le Q-1$. Then

$$\begin{aligned} \tilde{x}_{n,k} \equiv \tilde{x}_{n,Qm+q} &= \frac{1}{M} \sum_{\ell=0}^{M-1} \tilde{X}_{n,\ell} \mathrm{e}^{\mathrm{j}\frac{2\pi\ell k}{M}} \\ &= \frac{1}{QN} \sum_{\ell=0}^{N-1} X_{n,\ell} \mathrm{e}^{\mathrm{j}\frac{2\pi\ell(Qm+q)}{QN}}. \end{aligned} \tag{10.89}$$

If $q = 0$, then

$$\begin{aligned} \tilde{x}_{n,k} \equiv \tilde{x}_{n,Qm} &= \frac{1}{Q} \left(\frac{1}{N} \sum_{\ell=0}^{N-1} X_{n,\ell} \mathrm{e}^{\mathrm{j}\frac{2\pi\ell Qm}{QN}} \right) \\ &= \frac{1}{Q} \left(\frac{1}{N} \sum_{\ell=0}^{N-1} X_{n,\ell} \mathrm{e}^{\mathrm{j}\frac{2\pi\ell m}{N}} \right) \\ &= \frac{1}{Q} x_{\mathrm{n},m}. \end{aligned} \tag{10.90}$$

If $q \neq 0$, then using

$$X_{n,\ell} = \sum_{i=0}^{N-1} x_{\mathrm{n},i} \mathrm{e}^{\mathrm{j}\frac{2\pi i\ell}{N}}, \tag{10.91}$$

in (10.89) gives [188]

$$\tilde{x}_{n,k} \equiv \tilde{x}_{n,Qm+q} = \frac{1}{Q}\left(1 - \mathrm{e}^{\mathrm{j}2\pi\frac{q}{Q}}\right)\frac{1}{N}\sum_{i=0}^{N-1}\frac{x_{\mathrm{n},i}}{1 - \mathrm{e}^{\mathrm{j}2\pi\left(\frac{m-p}{N}+\frac{q}{QN}\right)}}. \tag{10.92}$$

It follows that the time-domain vector $\tilde{\mathbf{x}}_n$ has an exact copy of the time-domain vector $\mathbf{x}_n$ in N coordinates defined by $k = Qm,\ 0 \leq m \leq N-1$. In between these positions, the vector $\tilde{\mathbf{x}}_n$ has values that depend on a complex weighted sum of all the time-domain symbols in the time-domain vector $\mathbf{x}_n$. This will increase the PAPR significantly.

L-OFDMA is the scheme adopted in 3GPP LTE. While it may seem that L-OFDMA is less desirable due to the high PAPR, the waveform is less sensitive to frequency offsets and phase noise, as compared to I-OFDMA. While it may seem that L-OFDMA also looses the diversity advantages of I-OFDMA, it may be possible that all sub-carriers fade together and only one channel estimator is needed.

Cyclic Guard Interval and SC-FDE

After performing sub-carrier mapping, the transmitter inserts a cyclic guard interval of length-G, such that G equals or exceeds the maximum expected discrete-time channel length L. The purpose of the cyclic guard interval is to isolate the transmitted blocks and to permit SC-FDE at the receiver as discussed in Sect. 10.2. Here we assume a length-G cyclic prefix. The cyclic prefix is added to the sequence $\tilde{\mathbf{x}}_n = \{\tilde{x}_{n,m}, m = 0,\ldots,M-1\}$ by simply copying the last G symbols of $\tilde{\mathbf{x}}_n$ and appending them to the beginning of $\tilde{\mathbf{x}}_n$. The symbol sequence with guard interval, denoted as $\tilde{\mathbf{x}}_n^g = \{\tilde{x}_{n,m}^g\}$, is

$$\tilde{\mathbf{x}}_n^g = \{\tilde{x}_{n,(m)_M},\ m = -G, -G+1, \cdots, -1, 0, 1, \cdots, M-1\}, \tag{10.93}$$

where $(m)_M$ is the residue of m modulo-M. When a cyclic guard is appended, the time-domain output symbols $\tilde{x}_{n,m}^g$ have duration $\tilde{T}_{\mathrm{s}}^g = (M/(M+G))\tilde{T}_{\mathrm{s}} = (N/(M+G))T_{\mathrm{s}}$ seconds.

Once the cyclic guard is removed and a DFT taken on the received block, SC-FDE can be applied. Typically, either a zero-forcing (ZF) or minimum mean square error (MMSE) SC-FDE is used. The required algorithms are described in detail in Sect. 10.2 and are not repeated here. ZF-FDE and MMSE-FDE can be applied to OFDMA as well, but there are better solutions. These include MRC for flat fading AWGN channels, and optimum combining (OC) with receiver antenna diversity. With OC, we maximize the signal-to-interference-plus-noise ratio for a flat faded desired signal in the presence of one or more flat faded and dominant co-channel interferers.

10.4.1 Peak-to-Average Power Ratio

One of the biggest advantages of SC-FDMA is its low PAPR. The PAPR for block n can be defined in terms of the discrete-time SC-FDMA samples as

$$\text{PAPR}_n = \frac{\max_m\{|\tilde{x}^g_{n,m}|^2}{(M+G)^{-1}\sum_{n=-G}^{M-1}|\tilde{x}^g_{n,m}|^2}. \tag{10.94}$$

The PAPR in this case depends only on the modulation signal constellation and sub-carrier mapping. With SC-FDMA pulse shaping can be used to reduce the PAPR and to reduce out-of-band emissions. Since each user in the SC-FDMA uplink uses only a subset of the sub-carriers, different approaches for implementing the pulse shaping have been suggested. With the conventional approach, the sample sequence $\tilde{\mathbf{x}}^g_n$ is transmitted using an amplitude shaping pulse $h_\text{a}(t)$ such that the continuous-time complex envelope corresponding to the nth block is

$$\tilde{s}_n(t) = \sum_{m=0}^{M+G-1} \tilde{x}^g_{n,m} h_\text{a}(t - m\tilde{T}^g_\text{s}). \tag{10.95}$$

For the continuous-time complex envelope $\tilde{s}_n(t)$, the PAPR for block n is defined as

$$\text{PAPR}_n = \frac{\max_{0\le t\le (M+G)\tilde{T}^g_\text{s}}|\tilde{s}_n(t)|^2}{\frac{1}{(M+G)\tilde{T}^g_\text{s}}\int_0^{(M+G)\tilde{T}^g_\text{s}}|\tilde{s}_n(t)|^2\text{d}t}. \tag{10.96}$$

In this case, the PAPR depends not only on the modulation signal constellation and sub-carrier mapping, but also on the pulse shaping waveform $h_\text{a}(t)$ as well. For SC-FDMA, the shaping pulse $h_\text{a}(t)$ can be chosen to be a frequency-domain root raised cosine pulse, since receiver matched filtering will yield an overall raised cosine pulse that satisfies the first Nyquist criterion for ISI free transmission. The required magnitude response is given by $|H_a(f)| = \sqrt{\tilde{T}^g_\text{s}}|P(f)|^{1/2}$, where $P(f)$ is the spectral raised cosine pulse defined in (4.47) with $T = \tilde{T}^g_\text{s}$. The root raised cosine filtering can be implemented either in the time-domain or the frequency-domain. With time-domain filtering, the sequence $\tilde{x}_{n,m}$ is passed through a digital filter $h_{a,n}$ having the corresponding analog filter impulse response $h_\text{a}(t)$ in (4.50) with $T = \tilde{T}^g_\text{s}$. Implementation of the root raised cosine time-domain filter requires that the sequence $\tilde{\mathbf{x}}^g_n = \{\tilde{x}_{n,m}\}_{m=-G}^{M-1}$ be upsampled prior to filtering, since the bandwidth of the root raised cosine pulse exceeds the Nyquist frequency $1/2\tilde{T}^g_\text{s}$. Assuming an upsampling factor of F, the upsampled sequence is

$$\tilde{x}^u_{n,\ell} = \begin{cases} \tilde{x}_{n,\ell/F}, & \ell = k\cdot F,\ k \text{ an integer}, \\ 0, & \text{otherwise}. \end{cases} \tag{10.97}$$

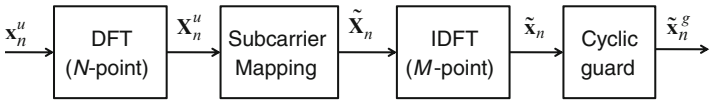

Fig. 10.24 SC-FDMA with frequency-domain root raised cosine filtering

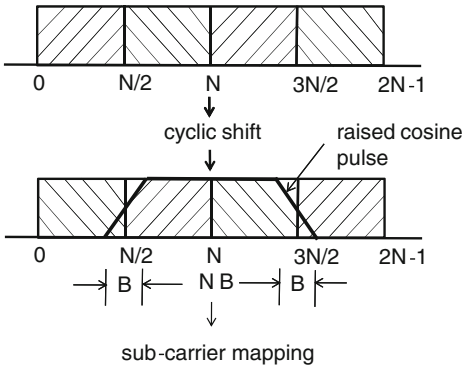

Fig. 10.25 Frequency-domain root raised cosine filtering

If the roll-off factor β lies in the range $0 \leq \beta \leq 1$, then an upsampling factor $F = 2$ will suffice. The upsampled digital filter impulse response in this case is given by $h_{a,n}^u = h_a(n\tilde{T}_s^g/F)$, where $h_a(t)$ is defined in (4.50) with $T = \tilde{T}_s^g$.

An entirely different approach is to implement the root raised cosine filtering in the frequency-domain. This approach is feasible with SC-FDMA because of the DFT/IDFT processing that is used in the transmitter. Figure 10.24 shows a transmitter block diagram for SC-FDMA with a spectrum shaping filter in the frequency-domain. As before, a block of data symbols $\mathbf{x}_n = (x_{n,1}, x_{n,2}, \ldots, x_{n,N})$ is input to an N-point DFT to yield the length-N vector $\mathbf{X}_n = (X_{n,1}, X_{n,2}, \ldots, X_{n,N})$. Once again, implementation of the root raised cosine filtering requires that the input sequence $\mathbf{x}_n$ be upsampled by a factor of F to yield the sequence $\mathbf{x}_n^u = \{x_{n,\ell}^u\}$, where

$$x_{n,\ell}^u = \begin{cases} x_{n,\ell/F}, & \ell = k \cdot F, \ k \text{ an integer}, \\ 0, & \text{otherwise}. \end{cases} \tag{10.98}$$

Rather than implementing the upsampling process in the time-domain, the upsampling process can be emulated in the discrete frequency-domain by generating periodic replicas of the vector $\mathbf{X}_n$, that is,

$$X_{n,\ell N+m}^u = X_{n,m}, \ \ \ell = 0, \ldots, F-1, \ \ 0 \leq m \leq N-1. \tag{10.99}$$

Once again, if the roll-off factor β lies in the range $0 \leq \beta \leq 1$, then an upsampling factor $F = 2$ will suffice, and we assume this value here. We then apply a cyclic shift of $N/2$ positions to the vector $\mathbf{X}_n^u$ and, afterwards, apply frequency-domain raised cosine filtering to generate the vector $\mathbf{X}_n^{sh}$ as shown in Fig. 10.25. After filtering, the sub-carrier mapping is applied.

The required frequency-domain pulse description can be obtained by modifying the pulse description in (10.76), where the subscript k now refers to the sub-carrier frequency. The pulse defined in (10.76) begins at index $k = 0$ and ends at $k = M + G - 1$. However, the block size should be set to N rather than M, and the guard interval in this case serves only to contain the required bandwidth expansion, which is equal to B. Hence, we set $M = N$ and $G = B$ in (10.76) to give

$$W_k^{\text{rc}} = \begin{cases} \sqrt{\frac{1}{2} + \frac{1}{2}\sin\left(\frac{\pi}{B}\left(k - \frac{B-1}{2}\right)\right)}, & 0 \le k < B, \\ 1, & B \le k < N, \\ \sqrt{\frac{1}{2} - \frac{1}{2}\sin\left(\frac{\pi}{B}\left(k - N + \frac{B+1}{2}\right)\right)}, & N \le k \le N + B - 1, \\ 0, & \text{elsewhere.} \end{cases} \tag{10.100}$$

The pulse in (10.100) has a flat-top of length $N - B$, and two roll-off sections of length B. We just need to relate the parameters B and N to the roll-off factor β used in the continuous-time root-raised cosine pulse description. The required values can be obtained by noting that $B = \beta/\tilde{T}_s^g$ and that the flat top portion has width $N - B = (1-\beta)/\tilde{T}_s^g$ and, hence, we choose B according to $\beta = B/N$. The required frequency-domain description can be obtained by right-shifting the pulse in (10.100) by $N - (N+B)/2$ positions.

Note that the overall length of the frequency-domain root-raised cosine pulse is $N + B$. Hence, with root-raised cosine filtering there are $N + B$ samples that are applied to the sub-carrier mapping, as opposed to just N samples without frequency-domain filtering. The extra B frequency-domain samples per user is the bandwidth cost that is required to implement the root-raised cosine filtering.

Problems

10.1. Consider an OFDM system having $N = 1{,}024$ sub-carriers that are spaced 4 kHz apart. Suppose that the waveform channel is a linear time-invariant channel consisting of two nonfaded equal rays spaced τ_d seconds apart, that is,

$$g(t, \tau) = g\delta(\tau) + g\delta(\tau_d),$$

where $g = \alpha e^{j\phi}$ is the gain associated with each of the two channel taps.

Find the value of the delay τ_d in the above channel model that will yield the worst possible bit error rate performance for this OFDM system.

10.2. Suppose that an OFDM system is implemented with a guard interval that is a cyclic extension of the IDFT coefficients as shown in (4.98).

(a) Show that the output of the OFDM demodulator is given by (10.6).
(b) Now suppose that the guard interval simply consists of a blank interval where nothing at all is transmitted. Assuming that $G \geq L > 0$ can the data block $\mathbf{x}_n$ be recovered by taking an DFT of the received block $\mathbf{R}_n = \{R_{n,m}\}_{m=0}^{N-1}$?

10.3. Assume the transmission of a known OFDM symbol, $\mathbf{c}_n = (c_{n,0}, \ldots, c_{n,N-1})$, given by the chirp sequence

$$c_{n,k} = \exp\left\{\mathrm{j}\frac{2\pi}{N}k^2\right\}, \quad 0 \leq k \leq N-1.$$

Coarse channel estimates can be obtained by computing

$$\begin{aligned}\tilde{T}_{n,i} &= \frac{z_{n,i}}{c_{n,i}} \\ &= T_{n,i} + \tilde{n}_{n,i}, \quad i = 0, \ldots, N-1,\end{aligned}$$

where $\tilde{\mathbf{n}}_n = \{\tilde{n}_{n,i}\}_{i=0}^{N-1}$ is a vector of independent and identically distributed complex Gaussian random variables with zero-mean and variance σ_n^2. This yields the channel estimate $\tilde{\mathbf{T}}_n = \{\tilde{T}_{n,i}\}_{i=0}^{N-1}$. The receiver then computes the vector $\mathbf{v}_n = (v_{n,1}, \ldots, v_{n,N})$, where $\mathbf{v}_n = \mathrm{IDFT}[\mathbf{T}_\mathrm{n}]$. Afterwards, the $\{v_{n,m}\}_{m=0}^{N-1}$ are passed through a rectangular window to zero $v_{n,m}$, $m \geq G+1$, and a DFT is taken of the resulting sequence to yield the refined channel estimate $\bar{\mathbf{T}}_n = \{\bar{T}_{n,i}\}_{i=0}^{N-1}$, such that

$$\bar{T}_{n,i} = T_{n,i} + \overline{n}_{n,i}, \quad i = 0, \ldots, N-1.$$

Show that the noise components $\overline{n}_{n,i}$ are zero mean and have a variance equal to $\sigma_n^2 \frac{G+1}{N}$.

10.4. Derive the MMSE-FDE solution in (10.65).

10.5. Derive (10.92) for L-FDMA.